

Open dissipative seismic systems and ensembles of strong earthquakes: energy balance and entropy funnels

Samvel Ts. Akopian

Schmidt Institute of Physics of the Earth, Gruzinskaya str., 10-1 Moscow 123995, Russia. E-mail: sakopian@yandex.ru

Accepted 2015 February 24. Received 2015 February 24; in original form 2014 July 14

SUMMARY

A concept of seismic system (SS), which is responsible for the preparation of an ensemble of strong earthquakes, is considered as an open dissipative system exchanging energy and entropy with the environment. Open dissipative SS allow one to describe the equilibrium and non-equilibrium states of SS, and the lithosphere evolution under different plate tectonic settings on the basis of seismostatistics. Several new seismic parameters ('seismic temperature', 'seismic time', dissipation function, efficiency, inelastic energy, dynamical probability) are defined and proposed for better understanding and describing the dynamical processes. The Sakhalin SS is considered to illustrate the behaviour of proposed parameters. By analogy to Liouville's equation in thermodynamics, it is shown that there is no criterion of instability in the domain where the Gutenberg-Richter law is true. In the proposed approach, the instability origination and the formation of seismogenic structures in the lithosphere are based on the energy versus information entropy power law; the existence of 'time arrow' also proceeds from such a dependence. Application of energy and trajectory diagrams enables to describe the preparation of strong earthquakes within an ensemble in terms of slow and fast timescales. These diagrams help perform the spatiotemporal-energy monitoring of the instability origination in the lithosphere. It is shown that the information entropy parameter can serve as a measure of the unknown external energy flow into the system (this energy is supplied for the elastic radiation energy in the earthquake sources and for inelastic processes in the system volume). The property of the ensemble of strong earthquakes is periodically to restore the SS equilibrium state that enables to describe the SS energy balance. The results offer possibilities to estimate the fraction of inelastic energy released by the SS medium during the preparation and occurrence of seismic catastrophes. The construction of phase diagrams and 'entropy funnels' in the virtual space (with time, energy and entropy coordinates) can provide new opportunities for the visualization of undetectable processes leading to disastrous earthquakes.

Key words: Instability analysis; Probabilistic forecasting; Seismic cycle; Elasticity and anelasticity; Earthquake dynamics; Statistical seismology.

1 INTRODUCTION

In order to quantitatively describe the seismic processes and preparation of strong earthquakes in the real medium, the concept of seismic system (SS), and the physical parameters of a number of SS states and the seismic entropy were introduced (Akopian 1995a,b,c, 1998). The notions of the number of SS states and the seismic entropy are not less important than the seismic energy and stresses measured and used in seismology (Kasahara 1981). Later, the parameter of seismic entropy was introduced by other researchers (Main & Al-Kindy 2002; Al-Kindy & Main 2003). However, in contrast to the author's approach, it was done formally on the basis of the thermodynamical definition of entropy and using the Gutenberg-

Richter (GR) empirical law (Gutenberg & Richter 1954). When the theory of non-equilibrium statistical mechanics and disasters is applied to earthquakes, the GR law acts as a base (Main & Burton 1984; Barriere & Turcotte 1994; Rundle *et al.* 2000; Main & Naylor 2010; De Santis *et al.* 2011). Mechanical replacement of thermodynamical energy in the entropy definition by energy of earthquakes demands specification and the formulation of the new physical task, which arises in seismology as a result of such a replacement. Otherwise, there are many questions arise regarding the adequacy of the obtained models for describing the real processes of earthquake. As shown by (Akopian & Kocharian 2013) the SS instability is caused by the power law and strong earthquakes of certain energy levels within any given SS are grouped into ensembles. Ensembles

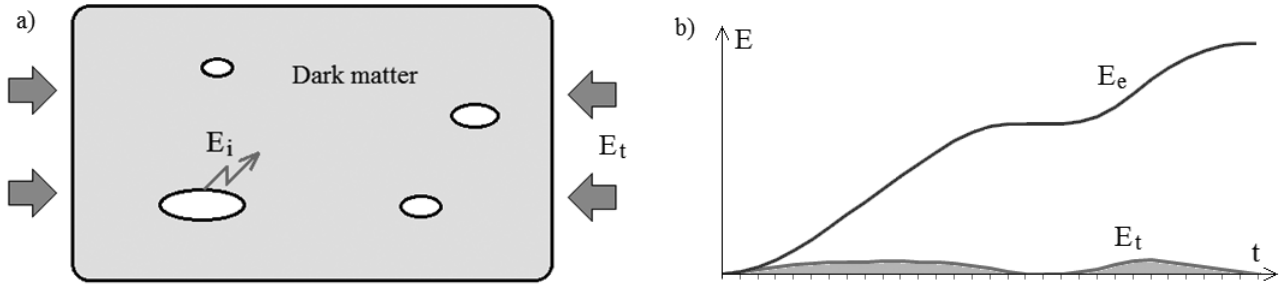


Figure 1. (a) SS as a ‘black box’ with sources of seismic energy E_i under compression setting. (b) The current and cumulative inflows of tectonic energy (E_t and E_e , respectively) into the system.

of strong earthquakes tend to fill seismic inhomogeneities within an SS over time. The SS macrostates are described by random indicator earthquakes of the magnitude range $M_h \leq M < M_{th}$, which play the main role in preparation of strong earthquakes with magnitudes more than the upper threshold, $M \geq M_{th}$. In seismology, earthquakes are usually classified into strong, moderate and weak in terms of radiated energy, intensity and structural damage, but the margin between them is rather conventional and ambiguous. In our approach, such terms as macro- and microstates of SS, strong earthquakes and indicator earthquakes become relative and depend on the SS size (configuration L on the surface and depth H) and the threshold parameters, M_h and M_{th} . The parameters of cumulative energy and entropy allow the seismic setting within an SS to be estimated at any moment of time. The method enables modelling and describing the dynamics of complex SS with internal inhomogeneities (including tectonic faults) and the prediction of the system behaviour with certain accuracy. The main statements of the seismic entropy method (Akopian 1995a,b,c, 1998, 2007) and the recent results (Akopian & Kocharian 2013) can be combined into a united theory where the SSs are considered as open dissipative systems exchanging energy and entropy with the environment (Prigogine 1980; Nicolis & Prigogine 1989).

In this work, the problems of equilibrium and non-equilibrium states and the applicability of the GR law to open dissipative SS are discussed. A set of physical parameters are introduced into seismostatistics to proceed from the theory of dissipative dynamical systems and the respective data to the SS concept. With the use of these parameters, the process of earthquake preparation is modelled in the form of spiral diagrams and entropy funnels which are unusual for modern seismology. The construction of the trajectory and energy diagrams describes the instability evolution and the energy balance restoration by strong earthquakes of an ensemble. The results are shown on the example of the Sakhalin SS (Akopian 1998; Akopian & Kocharian 2013), which is briefly described in Appendix A. Appendix B gives the examples of entropy funnels for the SSs of the Kuril-Kamchatka region.

2 OPEN SYSTEMS AND DISSIPATIVE STRUCTURES

2.1 Problem statement and difference from the viewpoint of classical mechanics

The main causes of earthquakes are located beyond the SS and associated with thermal convection in the upper mantle of the Earth (Turcotte & Schubert 1982). Therefore, we will consider the SS as an open dissipative system that exchanges energy, mass and heat with the environment. Since the dynamical processes of earthquake

preparation in the SS are relatively short term, such thermodynamical changes in the medium state as mass and heat exchanges will be neglected. The tectonic forces caused by plate motions lead to tension and deformations in the lithosphere and, in some local volumes of the geological medium, to rupturing with the release of elastic and inelastic energies. However, stresses and deformations in large volumes of the lithosphere are not the parameters that can be reliably recorded for solving the problems of dynamics and instability origination.

The SS volume is considered as a ‘black box’, whose configurations L on the surface and in the depth are known, whereas the internal structure is either unknown or known in general. The parameters of cumulative seismic energy and entropy enable to describe the energy state of such a ‘black box’ in whole and the evolution of this state in time. Under the action of external compression, the main information about a ‘black box’ state is provided by the indicator earthquakes, seismic waves which are recorded by seismic networks and then processed (Fig. 1a). By analogy with cosmology, we call the geological environment between seismic sources ‘dark matter’ because it does not manifest itself in the form of radiating the seismic waves. In this sense, the predominant part of the Earth’s volume can be considered as ‘dark matter’. External forces acting on the system boundaries cause internal deformations in the SS volume, $d\mathfrak{V} = \sigma_{ik} du_{ik}$, which are unknown. The energy, which equals to this work in volume V per time unit, will be called the inflow of tectonic energy into the system at the current moment of time, E_t . By analogy to motions in plate tectonics, this value is continuous. The integral of E_t on time is denoted as E_e

$$E_e(T) = \int_0^T E_t dt \quad (1)$$

and is called the cumulative inflow of tectonic energy into the system for time T . At such a statement, the external load once applied to the SS remains until occurrence of a strong earthquake. The inflow of tectonic energy E_t into the system can increase or decrease over time (Fig. 1a), but the cumulative inflow of tectonic energy, E_e , does not decrease (Fig. 1b).

The temporal change in state of such a ‘black box’ (or SS) will be described by using the parameters and definitions proposed in (Akopian 1995a, 1998; Akopian & Kocharian 2013). Let us formulate the basic principles of this approach and discuss some differences between the approach and the mechanical systems in physics. Each earthquake can be described by a vector $(\phi_i, \lambda_i, h_i, t_i, E_i)$ in the 6-D space, with the characteristic spatiotemporal and energy coordinates: the latitude ϕ_i , the longitude λ_i , the focal depth h_i and the time t_i when an earthquake occurs. The radiated seismic energy E_i is determined by the earthquake magnitude M_i (Gutenberg &

Richter 1956):

$$\log E_i = \alpha + \gamma M_i, \quad (2)$$

where $\alpha = 4.8$ and $\gamma = 1.5$ are the parameters and energy is measured in Joules. The spatial location of a rupture is usually the point at the hypocentre depth on a fault where the rupture has been nucleated at the time of its first dynamic motion. The accepted (simplified) model of an earthquake, a point source of radiated seismic energy in space, is sufficient to solve the problems raised in this paper. Therefore, volume characteristics of the source (faulting, focal mechanisms and so on) are neglected. The SS is also characterized by the threshold magnitude M_{th} . All earthquakes with magnitudes greater than or equal to the threshold one, $M \geq M_{\text{th}}$, are called strong and earthquakes with magnitudes $M_{\text{min}} \leq M < M_{\text{th}}$ are considered to be indicator earthquakes, where M_{min} is the minimal value among all representative earthquakes in a regional catalogue.

The time interval between two successive strong earthquakes in the SS, $T_j = t_j - t_{j-1}$, is labelled a seismic cycle, where t_j and t_{j-1} denote the times when two consecutive strong earthquakes occur. Hereafter, all the varying parameters within the seismic cycles are denoted by the subscript i , while the seismic cycles are numbered by j ($j = 1, 2, \dots, N$), where N is the number of realized seismic cycles, that is, the number of strong earthquakes. The current time interval T within any seismic cycle j is equal to $T = t - t_{j-1}$, with t_0 being the starting date of the first cycle. Suppose that $N - 1$ cycles were accomplished at time t starting from some initial date of observation t_0 . The total released energy in the SS within seismic cycles (after each strong earthquake) is defined by the parameter of cumulative energy E_c , which equals the total radiated energy of all indicator earthquakes registered up to any given time, t :

$$E_c(t) = \sum_{i=1}^{\tilde{N}(t)} E_i, \quad (3)$$

where a summation includes all indicator earthquakes $\tilde{N}(t)$ for a given time t with energies $E_i \geq E_{\text{min}}$ in a volume V of SS as recorded after the last strong earthquake t_{N-1} . In contrast to statistical physics (Landau & Lifshits 1980), such approach allows to exclude the spatial distribution of sources (in statistical physics, the distribution function) within the system volume from consideration and considers the time-dependent energy state of the entire system. Below, the spatial characteristics of indicator earthquakes in the SS volume will be omitted for simplicity. The scheme of $E_c(t)$ calculation after the occurrence of a hypothetical strong earthquake at time t_0 is shown in Fig. 2. For time description of the system state a new parameter $S_N(t)$ is introduced, which is analogous to action in Newtonian mechanics:

$$S_N(t) = (t - t_{N-1})E_c - \sum_{i=1}^{\tilde{N}(t)} (t_i - t_{N-1})E_i, \quad (4)$$

where t_i and E_i are the indicator earthquake occurrence time and radiated seismic energy, respectively. The parameter t_{N-1} is the time of occurrence of the last strong earthquake. The expression (4) at current time $T = t - t_{j-1}$ within any cycle j can be reduced to the more compact form:

$$S = TE_c - \sum_{i=1}^{\tilde{N}} T_i E_i, \quad (0 \leq T_i < T). \quad (5)$$

At fixed cumulative energy E_c in (5), $S_{\max} = E_c T$ and $S_{\min} = E_c$. The former corresponds to the case when the one ($\tilde{N} = 1$) hypothetical earthquake with the energy $E_1 = E_c$ occurs in the system at the

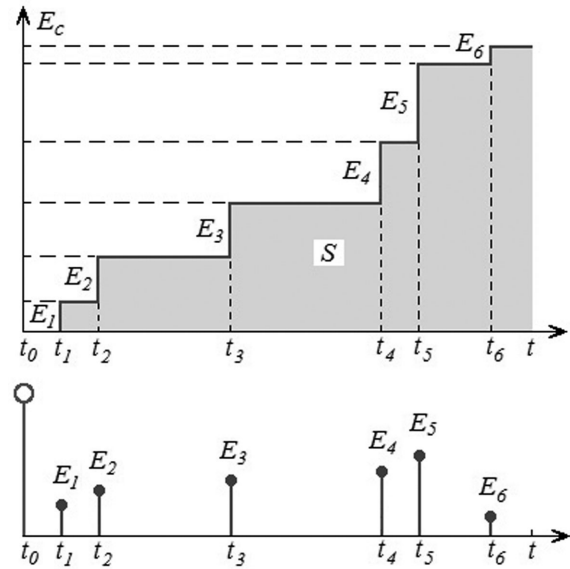


Figure 2. A schematic picture of a stepwise increase of the cumulative energy $E_c(t)$ function versus time within the first seismic cycle, beginning from time t_0 of a hypothetical strong earthquake. The energy values E_i and corresponding time occurrences t_i ($i = 1 \div 6$) of the six indicator earthquakes are also shown. The parameter $S(t)$ is equal to the total area beneath the cumulative energy function $E_c(t)$.

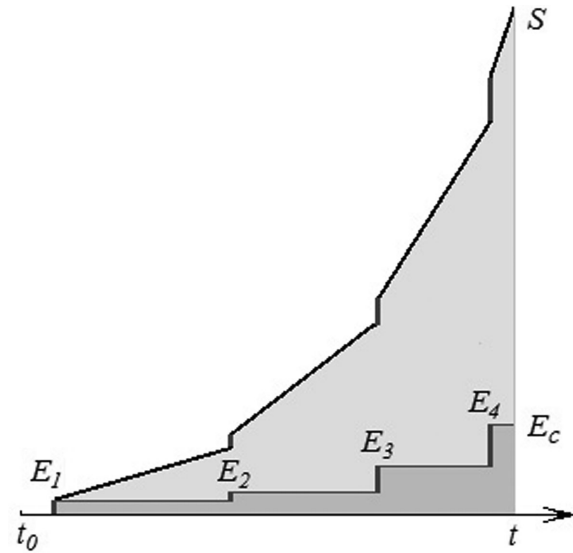


Figure 3. The rapid growth of the parameter $S(t)$ is compared to the stepwise increase of the cumulative energy, $E_c(t)$. The cumulative energy controls the rate of change of $S(t)$ in time, and any new indicator earthquake leads to a slope increase. The values E_i ($i = 1 \div 4$) are the energy of the four indicator earthquakes.

beginning of the cycle ($T_1 = 0$); the latter corresponds to the case when such an earthquake occurs in the end of the seismic cycle ($T_1 = T - 1$). Mathematically, integral parameter $S(t)$, as shown in Fig. 2, describes the area beneath the cumulative energy function $E_c(t)$ plotted versus time. Fig. 3 illustrates the comparative behaviour of the SS parameters $E_c(t)$ and $S(t)$. The seismic parameter $S(t)$ shows significant rapid growth in comparison with the stepwise increase in cumulative energy. The cumulative parameter $E_c(t)$ controls the rate of change in $S(t)$, and any new indicator earthquake inevitably leads to the increase in slope of the function $S(t)$. Therefore, both

$S(t)$ and $E_c(t)$ parameters are non-descending functions of time. For convenience and in order to avoid the complications caused by large numbers in seismology, let us apply the respective decimal logarithmic scales for (3) and (4)

$$K_c(t) = \log E_c(t), \quad W(t) = \log S(t), \quad (6)$$

where K_c is the cumulative energy class of indicator earthquakes and W is the seismic entropy, analogous to physical entropy in thermodynamics. The cumulativeness keeps the time memory of past behaviour and the sequence order of past earthquake events. In practice, these parameters are very reliable and can be easily calculated on the basis of earthquake data provided by existing catalogues. Therefore, at any time within the seismic cycle, the state of the SS ('black box') is determined by the pair of parameters E_c and S (or K_c and W). The plots of parameters E_c and W in the seismic cycles of the SS Sakhalin are shown in Appendix A. The physical meaning of these parameters was discussed in (Akopian & Kocharyan 2013). To remind, for any given value of S , the number N of all possible cumulative energy states E_{ci} ($i = 1, 2, \dots, N$) of the SS always equals S ($N = S$). It is significant that the entropy W of the SS, as in classical statistics, is defined with the accuracy of up to an additive constant depending on the choice of measurement unit (Landau & Lifshits 1980; Akopian 1995a). Introducing the state quantum of the SS ($h_s = E_h \delta t$) allows us to define seismic entropy as a dimensionless quantity with a specific value

$$W = \log \frac{S}{h_s}. \quad (7)$$

Introduction of the state quantum h_s (single microearthquakes) is related to the accuracy of measurements and the dimensions of SS. This means that we cannot specify S to an accuracy greater than our experimental error. As known in seismology potential energy of deformations larger than $\epsilon = 10^{-4} \text{ J cm}^{-3}$ cannot be accumulated in a unit rock volume (Tsuboi 1956). This restriction and the choice of the minimum time step $\delta t = 1$ lead to the choice of $h_s = 1 \text{ J s}$, which corresponds to the energy of a microearthquake with magnitude $M_h = -3.2$, the length of rupture $l_h \simeq 22 \text{ cm}$ and the volume of the source (l_h)³. In other words, the accuracy of measurements, energy restrictions and scale of a task in seismology (by analogy with the principle of uncertainty in quantum mechanics) set a lower limit on earthquakes (in sense of the lowest energy value). As a result of introduction of quantum, the parameters describing the system state become discrete. Discreteness of parameters allows us to avoid the appearance of infinitely large and infinitesimal numbers on the finite time intervals.

The definition of SS state essentially differs from that of the condition of a mechanical system. In the classical mechanics, the system consists of N material points in space. Simultaneous assignment of all generalized coordinates q_i and velocities \dot{q}_i determines the position of the system and allows to predict further movement of the system in time based on the principle of least action. The movement of the system is mathematically described by differential equations of the second order including the functions $q(t)$, whose integration allows the trajectories of mechanical system motion to be defined. As a result, such an approach complicates the task. The action of mechanical system (in terms of the Hamiltonian) for the conservation of energy ($E = \text{const}$) along the path from t_0 to t can be written as follows (Landau & Lifshits 1976):

$$S = -E(t - t_0) + \int_{t_0}^t \sum_{i=1}^N p_i dq_i, \quad (8)$$

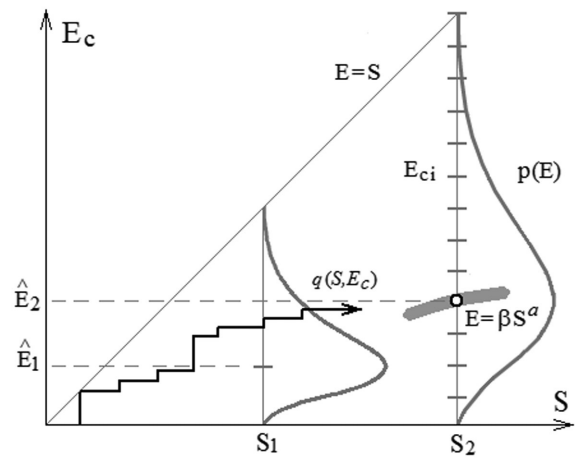


Figure 4. A scheme of the trajectory diagram. \hat{E}_1 and \hat{E}_2 are the most probable values of the cumulative energy for the states of S_1 and S_2 , respectively. E_{ci} is the number of various discrete values (levels) of cumulative energy at S_2 , $p(E)$ is the function of probability distribution in the interval $E \in [1, S_2]$. Thick arc shows the instability region of $E = \beta S^\alpha$, which attracts the trajectory.

were p_i and q_i are the canonical momenta and the coordinates of the material points, respectively. Although the eqs (5) and (8) are similar in appearance and have the same dimension (*energy × time*), they essentially differ from each other in contents. The seismic action differs in sign from the mechanical one, since the eq. (5) describes the change (development) of an open system, whereas the action in eq. (8) describes the motion over the space of a closed conservative mechanical system. In contrast to classical physics, the parameters (3) and (5) describe a number of possible states not of separate particles, but of the entire system at the current time, taking into account the entire history of the SS evolution. Holistic behaviour of the system as a selective volume of the lithosphere significantly alters the meanings of space and time. The systems are not eternal: they originate, evolve and, when all connections are destroyed, fade out. As a result of simplification, the description of SS state is provided by smaller number of parameters, compared to classical mechanics, that is in less detail. There are some similarities between our approach and the definition of a statistical system (Landau & Lifshits 1980). The statistical state of an entire closed system at rest (in the absence of translational and rotational movements) depends only on energy. From the seven additive independent integrals of motion (the energy, three components of the impulse vector and three components of the angular momentum), which completely determine the statistical properties of the closed system, only the energy remains. In our approach, the system is open hence the internal energy is not the integral of motion (it does not constant) and it becomes dependent on time. In other words both the time and the energy become the independent parameters describing the state of the system.

The motion trajectory of mechanical systems agrees with the least action principle (Lagrangian approach, Landau & Lifshits 1976). The trajectory of SS state is determined by the moving point $q(t) = q(S, E_c)$ on trajectory diagram (Fig. 4). Each jump-like interval that can be seen on the trajectory diagram corresponds to an indicator earthquake. At the beginning of a seismic cycle, the trajectory develops chaotically. Some cooperation appears between the parameters S and E_c over time and the trajectory starts to follow the power law (it gravitates to the most probable

energy state in Fig. 4)

$$E_c(t) = \beta(S)^a, \quad (9)$$

where E_c describes the most probable cumulative energy states of indicator earthquakes in the volume V at any given moment of time. If the law (9) is satisfied in all seismic cycles for the same constants a and β , then strong earthquakes in the SS volume are combined into an ensemble and form independent seismic cycles. The probability distribution of the energy states (which is the result of some energy states degeneration) determines the information entropy (Akopian 1995a; Akopian & Kocharian 2013)

$$\langle W \rangle = - \sum_{i=1}^S p_i \log(p_i), \quad (10)$$

where

$$p_i = \frac{m_i}{n}, \quad 0 < p_i < 1, \quad \sum_{i=1}^S p_i = 1. \quad (11)$$

Here, n is the number of all possible paths (trajectories) to the state $q(E_{ci}, S)$, $i = 1, 2, \dots, S$ ($n > S$); m_i is the degree of the degeneration of the current energy state E_{ci} (this degree equals the number of possible trajectories which can lead the system to the state E_{ci}). Therefore, the degeneration of the energy states actually increases the level of their ‘attendance’ and makes these states more probable. The probability distribution function $p(E)$ for a given S , being defined for any limited interval $E \in [1, S]$ (Fig. 4), is close to the Poisson distribution

$$p(E) = \frac{1}{E!} (\hat{E})^E e^{-\hat{E}}, \quad (12)$$

where \hat{E} is the most probable value of the cumulative energy. The distribution (12) differs from the Poisson one by the normalization condition (11), where the sum is finite. So, in contrast to the systems in classical mechanics, describing the movement of particles (or, in the case of quantum mechanics, describing the states of atoms and molecules), our approach describes the evolution of the entire system on the basis of time, cumulative energy and information entropy.

Back to the problem statement, note that the rigid body in the SS volume should be considered as a superposition of independent seismic sources in order to exclude the stresses and deformations within a ‘black box’, analogous to how it is done in integrable systems (Goldstein 1950; Landau & Lifshits 1980). In such an approach energy is not separated into kinetic and potential. The description of the potential energy accumulated before the strong earthquake and reflecting the complex interaction between fault structures, of course, complicates the task. Excluding the potential energy from the consideration and replacing the kinetic energy of the displacement in seismic sources by the radiation energy give an opportunity for a new understanding of the system dynamics, allowing us to consider the medium in the form of discrete sources of energy which, in contrast to stress, can be reliably recorded (measured) by instruments. In terms of physics of the Earth and for the purpose of earthquake monitoring and earthquake prediction on the basis of seismostatistics, we have to make a choice in favour of the energy approach, because the record of distributions of stress and deformation within large SS volumes with the desired time step is almost impossible. Nevertheless, recording of the earthquake parameters by seismic networks around the world (starting from a certain threshold magnitude) is already a solved problem. In such case, we obviously cannot directly take into account the mechanical

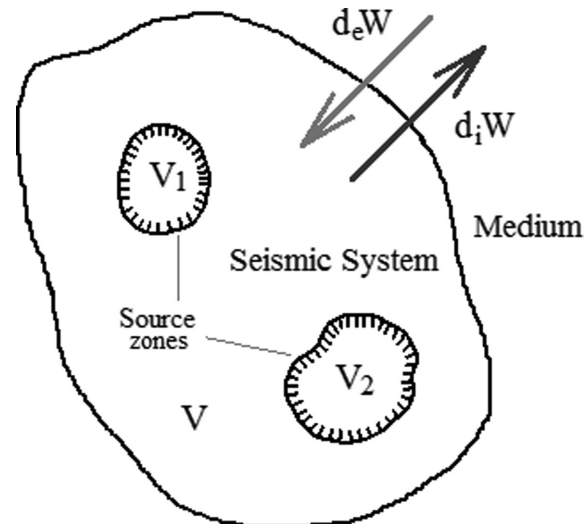


Figure 5. Schematic representation of an open SS with volume V , exchanging entropy with the environment (shown by arrows). V_1 and V_2 are the source zones of earthquakes.

energy of interaction between individual structural elements of seismic sources. However, the energy of such interaction is indirectly available in our approach and it is this energy that causes an ensemble of strong earthquakes in SS (Akopian & Kocharian 2013). Lacking the necessary information about the state of the medium (‘dark matter’), we can observe only the discrete reaction of the medium to an external continuous effect. When modelling the dynamical behaviour of such a medium based on the reliably recorded parameters (3) and (4), it is possible to solve a complex problem of the critical behaviour of dissipative structures in discrete volumes of the geological medium.

So we have the ‘black box’ (SS) with the unknown internal structure (‘dark matter’), the boundary conditions, and the information about internal seismic sources. The problem is to construct the theory that would describe the origin of seismic instability within the system and would estimate the balance of elastic and inelastic energy in a SS on the basis of this information. In fact, it is necessary to solve a fundamental problem of seismology: the problem of the estimation and control of the energy coming into the open SS.

2.2 SSs as open dissipative systems

Fig. 5 shows the scheme of an open dissipative SS interacting with the environment. According to the ideas from (Prigogine 1980; Nicolis & Prigogine 1989; Akopian 1998), the entropy change in an open SS can be written as

$$dW = d_iW + d_eW, \quad (13)$$

where d_iW is the internal entropy production from an earthquake occurrence (this parameter is always positive), and d_eW is related to the inflow and outflow of tectonic entropy in the SS (subscripts near the differential should not be confused with the summation index). Of course, the mathematical notation d_iW is somewhat arbitrary, as it means continuity and differentiability of the function W . Since the entropy is an additive quantity, piecewise differentiable with the first-order discontinuities (Rade & Westergren 2004), the value of $W(T)$, calculated in the seismic cycle, is the change of entropy from the beginning of the seismic cycle, $W(T) = \Delta W = \int_0^T dW$, in so far as $W(0) = 0$. Therefore, the behaviour of infinitesimal

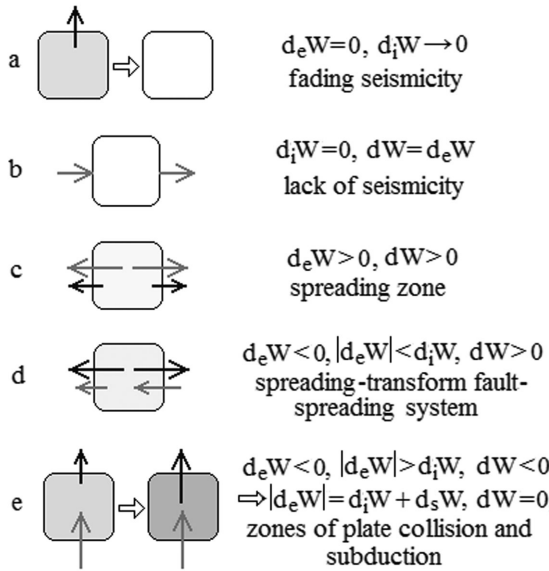


Figure 6. Schematic representation of entropy balance in an open SS under different seismotectonic settings. Squares denote SS; dark arrows, internal entropy production; light arrows, inflow and outflow. See the detailed explanations in the text.

dW reflects the nature of processes within the entire seismic cycle described by the entropy W . In this sense, dW is equivalent to W ($dW \equiv W$).

Depending on the specific tectonic conditions the sign of $d_e W$ can be either positive (outflow) or negative (inflow). The total change in the entropy of an open system according to eq. (13) may be positive, negative or zero. In a SS where active tectonic processes (i.e. earthquakes) take place, the entropy $d_i W$ is always produced. If a SS attains the state with $d_e W = 0$, then, by definition, $dW = d_i W \geq 0$. This corresponds to the case when an external influence stops and a seismic activity in the SS decreases (the system starts to discharge). Equality is attained when earthquakes completely discharge the system and no further activation takes place; that is the system attains an equilibrium with the environment (Fig. 6a). This pattern can be observed in long-time intervals, at the stage of the evolution along convergent boundaries after the collision of continental plates (for example, the boundary between Europe and Asia along the Ural Mountains). The previously active boundary slowly locks up and eventually loses seismic activity due to the rearrangement of convective cells in the mantle. The deceleration of convective flows supporting active processes leads to $d_e W \rightarrow 0$, and hence $d_i W \rightarrow 0$ (i.e. the system fades out). In small time intervals, these processes can take place after strong earthquakes of an ensemble. At the end of seismic cycles strong earthquakes relieve the main accumulated stress and reduced to zero aftershock activity finishes the process; the system temporarily turns to an equilibrium state.

If there is no entropy production in the SS, then $dW = 0$ and $dW = d_e W$; that is the system, remaining seismically quiet, will interact with the environment and transfer tectonic entropy from one medium to another. Such a pattern can be observed in cratonic areas within tectonic plates and blocks (Fig. 6b). This can lead to faulting and rare strong earthquakes in non-seismic areas between SSs.

The case when $d_e W > 0$ and $dW > 0$ can take place in a SS that includes a spreading zone, which is a source of dynamical processes in the system (Fig. 6c). In this case, internal tensions

cause the tectonic activity and earthquakes in a SS: a spreading system activates and pressures on the environment. Such a situation is observed at the Mid-Atlantic Ridge and in the areas of the rift zones origin (for example, the East African Rift Valley).

If $d_e W < 0$ and $|d_e W| < d_i W$, then $dW > 0$, and this is the case when the system is characterized by a spreading-transform fault-spreading structure (Fig. 6d): besides spreading zones, an extra internal seismic entropy production is related to the interaction between plates in the zone of transform fault. The relative motion rate for the boards of a transform fault is twice as big as the spreading rate (Turcotte & Schubert 1982).

The most interesting case is when

$$d_e W < 0 \text{ and } |d_e W| > d_i W, \text{ hence } dW < 0; \quad (14)$$

when the difference between the inflow and outflow of entropy goes down (but increases in absolute terms) and reaches the critical value

$$dW = d_i W + d_e W = d_k W < 0, \quad (15)$$

the system abruptly compensates this difference by an additional production, $d_i W \rightarrow d_i W + d_s W$, and restores the balance:

$$d_s W = -d_k W \text{ then } dW = 0. \quad (16)$$

The cases described by eqs (14)–(16) are periodically implemented for the SS located in compression zones (zones of plate collision and subduction, Fig. 6e). More than 90 per cent of the world's seismic energy is released in these zones. If the condition (16) is satisfied at each time step, it means that the SS consists of sliding (with a weak contact) or steady-motion blocks, which immediately react to an external load and turns the system into the equilibrium state. Such a situation can be observed in zones of creep. During the tectonic evolution of the Earth, at the considered time intervals of tens and hundreds of millions of years, the system can rearrange itself and pass from one stage to another. So if we consider the SS is linked with the tectonic plate without relative motion it is possible to describe the SS evolution over geological eras, when the movement of the lithosphere on the Earth's surface. On this consideration the SS is to evolve, passing the successive stages from a spreading zone to subduction (or continent-to-continent collision) in accord with the sequence $c \rightarrow d \rightarrow b \rightarrow e \rightarrow a$ shown in Fig. 6. In other words, in such a formulation of the problem the SS originates, then evolves and finally fades out. However, for practical purposes of the earthquake prediction, in the following sections we will consider the case e (Fig. 6) in the shorter time intervals (tens and hundreds of years), when the tectonic situation in a region does not change significantly.

The entropy production $d_i W$ is associated with the irreversible processes in a system. The entropy production in a SS showing no seismic activation will be called static, and that for a SS with an activated seismicity will be called dynamic. A static entropy production takes place permanently in the time intervals between discrete seismic events. At constant volume and mass of a SS, and with the use of formulas (3)–(6), let us find the rate of an internal entropy production (entropy production includes both static and dynamic):

$$\frac{d_i W}{dt} = \left. \frac{d_i W}{dt} \right|_{E_c=\text{const}} + \left. \frac{d_i W}{dt} \right|_{E_c+\Delta E} = \frac{E_c + \Delta E}{S \ln 10}. \quad (17)$$

The rate of internal seismic entropy production depends on the ratio between cumulative seismic energy of indicator earthquakes and density state function. At the moments corresponding to occurrences of indicator earthquakes ($t = t_k$), the cumulative energy

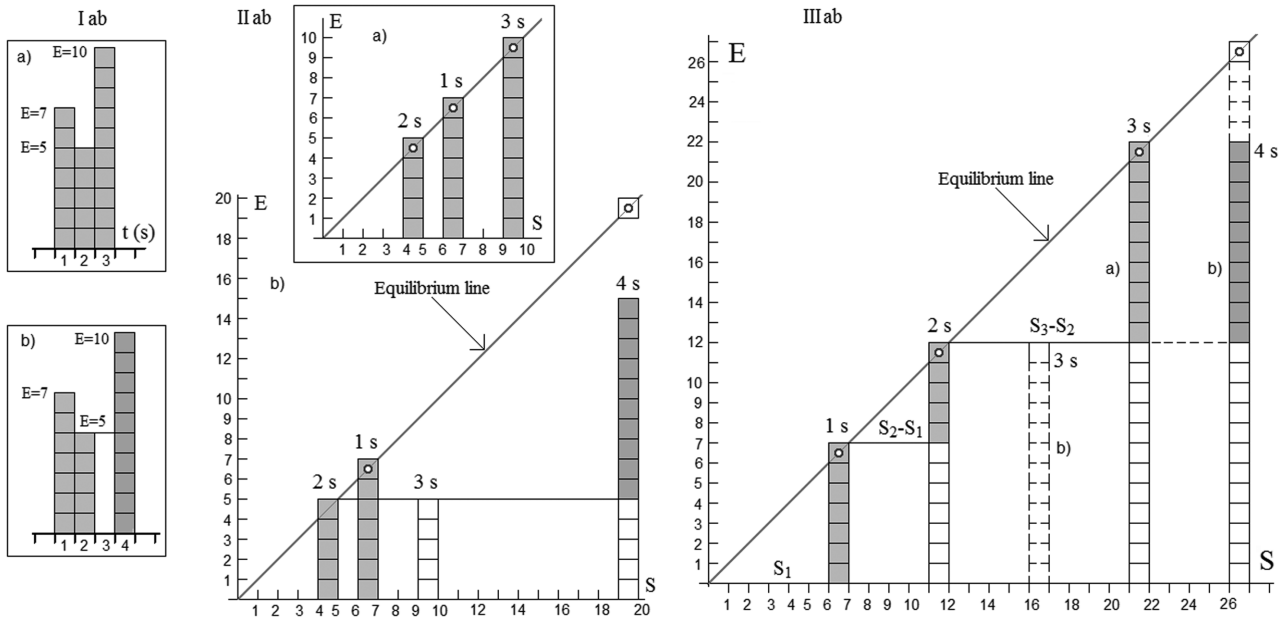


Figure 7. Two versions of seismic activity (Iab): (a) continuous, (b) with a ‘hiatus’ at 3 s. The respective trajectories on the trajectory diagram (IIab): (a) the system tends to the equilibrium after each earthquake, (b) after the second earthquake, the trajectory does not interrupt and deviates from the equilibrium line. The pattern of trajectories with the changes in the equilibrium states taken into account (IIIab): (a) the system tends to the new equilibrium state after each earthquake, (b) at 2 s, trajectory deviates from the equilibrium line. Small circles indicate that the trajectory is interrupted.

jump ΔE equals the elastic energy E_k of k th indicator earthquake ($\Delta E = E_k$), and the entropy production abruptly increases. At moments of indicator earthquakes t_k , the entropy production rate is not defined. Let us define it left and right of t_k

$$\frac{d_i W}{dt} \Big|_{t \rightarrow +t_k} = \frac{d_i W}{dt} \Big|_{t \rightarrow -t_k} \left(1 + \frac{E_k}{\sum_{i=1}^{k-1} E_i} \right). \quad (18)$$

Further, the value of entropy production rate at the moments of indicator earthquakes t_k will be assumed to be left of t_k .

Thus, when seismic entropy is produced, the tectonic force always exists; this force feeds the system with negative entropy, $d_e W < 0$, which is an unknown value, in principle. The macroscopic faulting process, a significant for a SS volume, is preceded by the decrease in open system’s entropy, in accord with the eq. (14). As soon as the difference between the outflow of entropy and its inner production attains a critical value, as described by the eq. (15), the system rapidly rearranges passing into a new equilibrium state through an intensive release of seismic energy (a strong earthquake) in a relatively short time interval. An open dissipative SS restores its order by formation of structural inhomogeneity (origination of a new fault). The many time repetition of seismic cycles during the millennia led to the formation of internal structural inhomogeneities (faults) and hence shaped the modern structure of the lithosphere.

2.3 Equilibrium and non-equilibrium states

Trajectories of the SS start from the equilibrium state after an indicator earthquake with the magnitude $M \geq M_h$ (Akopian & Kocharian 2013). Below we will, first, discuss the physical sense of the lower threshold magnitude M_h separating the equilibrium and non-equilibrium states, second, formulate the equilibrium state of a system and, third, show how this state depends on the chosen time step and the frequency of the earthquake recurrence. The minimal time step sufficient for describing the seismic processes is $\delta t = 1$ s

(Akopian 1995a). Enlargement of time step will be described by the parameter k ($k \geq 1$). If T_c (in seconds) is the duration of a seismic cycle, then the measure of duration will decrease as the time step enlarges ($t' \rightarrow k\delta t$), $T' = T_c/k$. For practical monitoring and earthquake prediction, the sufficient time step values are an hour, a day, a month and a year ($k = 3.6 \times 10^3, 8.6 \times 10^4, 2.6 \times 10^6, 3.2 \times 10^7$). The choice of minimal time step in the dynamics of ensemble of strong earthquakes depends on factual accuracy of earthquake magnitude definition, earthquakes duration and on number of finished seismic cycles. The chosen time step must be smaller than seismic cycle duration, $\delta t' \ll T_c$, at that.

To determine the equilibrium and non-equilibrium states on the trajectory diagram, let us consider a simple example. Two versions of seismic activity with energies of 7, 5 and 10 conventional units are shown in Fig. 7 (Iab). In the first case, quakes occur continuously at 1, 2 and 3 s; in the second case, with a ‘hiatus’ at 3 s. In continuous activation, we assume that at the each time step the system responds to external action by a quake and tends to the equilibrium. In Fig. 7 (IIab), the trajectories in a plane $\{S, E\}$ are given for these two cases. In the first case, after every time step, the trajectory will be interrupted on the equilibrium diagonal, in the points with coordinates $(7,7)$, $(5,5)$ and $(10,10)$ (these points are shown in Fig. 7, IIa). Usually, when the system tends to the equilibrium, the trajectory is terminated and a new path starts at the origin of coordinates. In the case IIb, the trajectory is not interrupted after 2 s due to missing activation at 3 s. As a result, the trajectory deviates from the equilibrium diagonal at 3 s, runs to the point $(10,5)$ and enters the non-equilibrium state at 4 s (in the point with $S = 20$ and $E = 15$). In Fig. 7, IIIab shows the trajectories of these two cases without transferring them to the origin of coordinates at the equilibrium states (the increment, $\Delta S_2 = S_2 - S_1 = 5$ and $\Delta S_3 = S_3 - S_2 = 10$ are added to each equilibrium state). Such a diagram shows the development of trajectory from the initial time point. With such a representation, at permanent (stationary) seismicity in each time step, the trajectory will grow stepwise, remaining on the diagonal line. Different

Table 1. Dependence of the equilibrium earthquake magnitude \bar{M}_{\max} on time step δt that equals the average recurrence period ($\delta T = \delta t/10^{7.5}$).

Time step	$\delta t(s)$	$\delta T(yr)$	$\bar{N} = 1/\delta T$	$\bar{N}/(yr)$	\bar{M}_{\max}
1 hr	$10^{3.56}$	$10^{-3.94}$	$10^{3.94}$	8760	1.2
1 d	$10^{4.93}$	$10^{-2.56}$	$10^{2.56}$	365	2.8
1 month	$10^{6.41}$	$10^{-1.08}$	$10^{1.08}$	12	4.5
3 months	$10^{6.89}$	$10^{-0.61}$	$10^{0.61}$	4	5.0
1 yr	$10^{7.50}$	1	1	1	5.7
5 yr	$10^{8.20}$	$10^{0.70}$	$10^{-0.70}$	0.2	6.5

equilibrium points on the diagonal line mean that the system suffers structural changes in these equilibrium states. After each quake, a new inhomogeneity (rupture, displacement) emerges in the system. Formally, in each equilibrium point on the diagonal line in Fig. 7, (IIIab), it is possible to come if a single hypothetical earthquake with the total energy $E_c = S$ occurs, so on the 2 s with $E_c = 12$, on the 3 s with $E_c = 22$. In the first case (frequent seismicity), the condition $d_i W = -d_e W$ is satisfied at each time step, that is the entropy inflow from beyond the system is completely supplied by internal production without losses and the system tends to the equilibrium, $dW = 0$. In the case of rare seismicity the system deviates from the equilibrium and becomes dissipative.

This example shows the importance of continuous seismic activity at each time step for SS state to be stable. Let us define an earthquake that occurs in SS one time per the chosen time step on average as the largest equilibrium earthquake with magnitude \bar{M}_{\max} . The system reaches to an unstable state and the process will become irreversible if an indicator earthquake with magnitude $M > \bar{M}_{\max}$ occurs at least at one time step. Since this moment, the trajectory on trajectory diagram starts. The value of \bar{M}_{\max} can be estimated from the earthquake recurrence frequency in the SS volume during a seismic cycle, using the GR law for j th seismic cycle:

$$\log \bar{N}_j(M) = \hat{a}_j - \hat{b}_j M, \quad (19)$$

where \bar{N}_j is the average annual number of earthquakes and $j = 1, 2, \dots$ is the number of finished seismic cycles. In (19) constants of the GR law are denoted by hats to distinguish them from constants of the power law (9). Magnitude \bar{M}_{\max} of the SS equilibrium state at fixed time step is found from the condition when at least one earthquake of this magnitude occurs at each time step (on average). Let δT be a time step measured in years ($\delta T = \delta t/k_y, k_y = 10^{7.5}$). Then let us choose an average recurrence period $\delta T = 1/\bar{N}$ (Lomnitz 1974). Using eq. (19), the value of maximal magnitude \bar{M}_{\max} of an equilibrium earthquake, depending on the time step, can be estimated as follows:

$$\bar{M}_{\max}(k) = \frac{\hat{a} - \log \frac{1}{\delta T(k)}}{\hat{b}}, \quad (20)$$

at $\delta T = 1$, $\bar{M}_{\max} = M_{\max}^* = \hat{a}/\hat{b}$. As an example, Table 1 shows the equilibrium magnitudes \bar{M}_{\max} for different time steps at $\hat{a} = 5.0$ and $\hat{b} = 0.88$.

The dependence of the equilibrium earthquake magnitude on the chosen time step (1, 3 and 12 months) is shown in Fig. 8. The time step reduction (increase in accuracy of monitoring and prediction) leads to the decrease in equilibrium magnitude. The characteristic deterministic timescale for the description of seismic processes is extremely large, varying from 1 s to millennia ($> 10^{10}$ s). Instrumental earthquake catalogues since 1900 enable to describe SS dynamics with time step from 3 to 1 month, while more representative catalogues since 1974 provide time step of up to about 10 d.

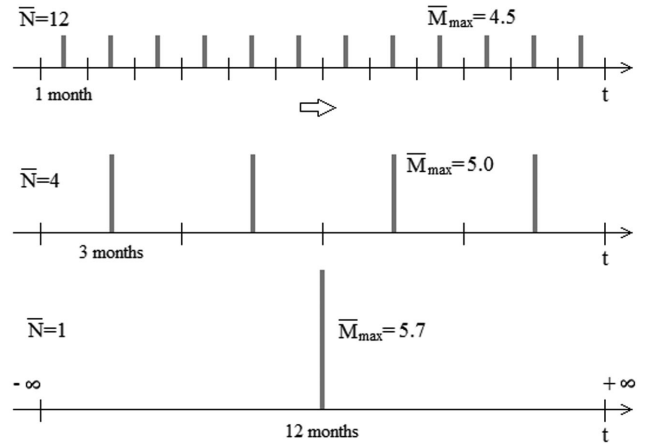


Figure 8. Dependence of equilibrium earthquake magnitude on time step duration (the chosen values are 1, 3 and 12 months).

When $\bar{N} < 1$, SS has to be described using large time steps (50, 100, 1000 yr) and high equilibrium magnitudes. The concept of dynamics at $\bar{M}_{\max} = 9.0$ loses its modern sense and only recurrence is left. Unfortunately, seismologists in their studies increase the averaging time step, trying to improve the statistics of seismicity and to enhance the recurrence law. Actually they are even more away from the real dynamical problem of earthquake preparation and affect the accuracy of monitoring over time. As is seen in Fig. 8 the equilibrium state is symmetric in any chosen time interval (time is reversible). If there are no additional external effects on the system, such a stable state will be kept in long time intervals. Let us show that the system state will be stable until seismicity exceeds the magnitude \bar{M}_{\max} .

Now let us consider the dynamics and non-equilibrium states. Additional external effect may lead to an earthquake with $M > \bar{M}_{\max}$ and appearance of time asymmetry. The simplest case of time asymmetry in SS with the time step of 1 month is exhibited in Fig. 9. The situation shown in Fig. 9(a) illustrates the case when an earthquake with energy $E > \bar{E}_{\max}$ occurs at the beginning of the year. Then, at the end of the year, the SS will attain the state with energy E and $S = 12E$. If to perform time reversal transform $t \rightarrow -t$ (Fig. 9b), an earthquake will occur at the end of the year and the system will attain another state (with $S = E$). It means violation of time symmetry. As is well known (Popper 1956, 1958; Prigogine 1980), it is precisely in the dissipative systems that where invariance of time violates and the ‘arrow of time’ appears. Our example shows that appearance of time asymmetry is not directly related to the parameter of cumulative seismic energy E and emerges when describing the SS state by parameter S . It means that dissipative properties of SS are described by the parameter S denoting the number of SS states (or by entropy W). Note that all real SSs are dissipative.

The main state of a SS at the microscopic level is assumed to be that with the single quantum $h = 1$ J s (Akopian 1995a). The quantum value for real systems can be chosen depending on time step and equilibrium earthquake energy by formula

$$\hbar = \bar{E}_{\max} \delta t. \quad (21)$$

For example, at $\bar{E}_{\max} = 10^{11.2}$ J ($M = 4.0$) and $\delta t = 1$ month, $\hbar = 10^{17.61} h$. Starting from that SS state, the indicator earthquake occur randomly and the energy distribution in the chosen time intervals becomes discrete and non-uniform. Let the number of all earthquakes with magnitudes $M_{\min} \leq M \leq \bar{M}_{\max}$ occurred during

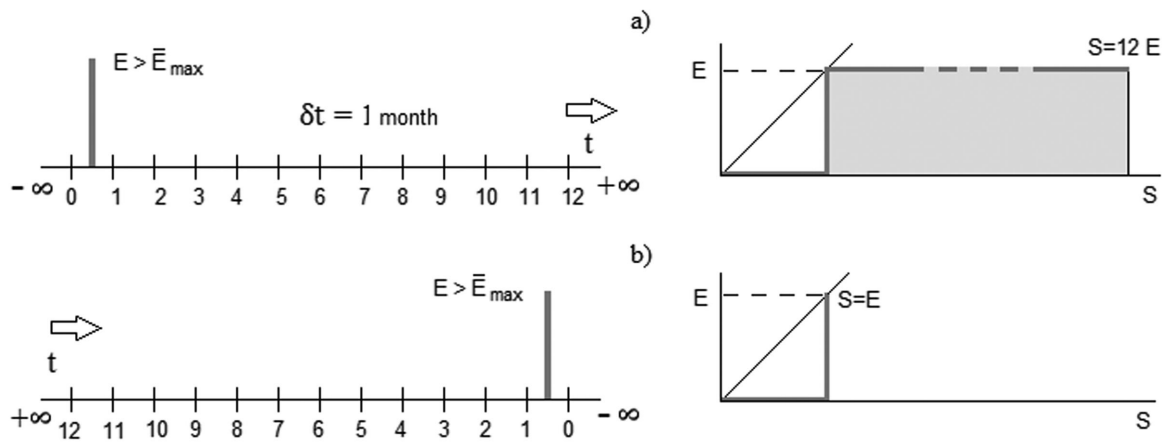


Figure 9. Example of time asymmetry in SS: (a) the system comes to a state $S = 12E$, (b) time reversal, system attains the state $S = E$.

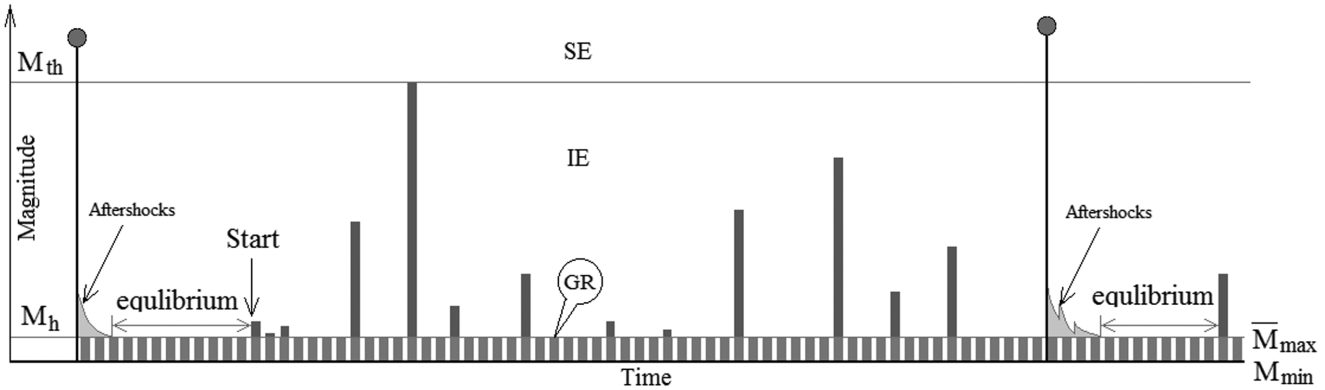


Figure 10. Hypothetical seismic cycle of a SS. SE means strong earthquakes, IE means an indicator earthquake, GR means background level (microseismicity domain where the GR law is true).

the time step δt be denoted by m_0 . This is the domain of earthquake magnitudes, where the GR law is true. Let the energy of these earthquakes be E_{mi} ($m = 1, \dots, m_0$), then their sum can be considered as one hypothetical background earthquake with total energy

$$E_i^{m_0} = \sum_{m=1}^{m_0} E_{mi}, \quad (22)$$

where E_{mi} is found from the formula $\log E_{mi}(J) = 4.8 + 1.5M_{mi}$ (Gutenberg & Richter 1956). Using the GR law for the average recurrence period of 1 month ($\bar{M}_{\max} = 4.5$), in the magnitude range of $2.0 \leq M \leq 4.5$ and at magnitude step $\Delta M = 0.2$, the energy of background earthquake $E_i^{m_0} \cong 2.0 \times 10^{12}$ J. The minimal magnitude M_h of the indicator earthquakes that lead to instability can be assumed to be

$$M_h = \bar{M}_{\max} + \Delta M, \quad (23)$$

then $M_h = 4.7$, $E_h = 0.5 \times 10^{12}$. In other words, the weakest indicator earthquakes will have the energy of about background one (total energy of all microquakes), $E_h \cong E_i^{m_0}$.

Fig. 10 shows the general scheme of seismicity during a hypothetical seismic cycle in a SS. There are three main levels of seismicity, separated by threshold magnitudes M_h and M_{th} . After a strong earthquake and decrease in aftershock activity, the system attains the equilibrium state that exists until the first non-equilibrium indicator earthquake. Equilibrium (background) level ($M < M_h$) uniformly fills all discrete time steps and includes microseismicity. The GR law is true at this level. In other words, there is no criterion

of instability in the domain where GR law is true. The GR law, like the Liouville's equation in thermodynamics (Prigogine 1980), does not describe neither the dynamics of deviations from stable state, nor that of instability appearance. Time reversible stationary processes at microscopic level (background microseismicity) do not play a key role in preparation of ensemble of strong earthquakes (SE domain in Fig. 10). They only characterize the minimal equilibrium time interval within the seismic cycle after the termination of aftershocks activity and before the disturbance of equilibrium. The deviation from equilibrium state (IE domain in Fig. 10) starts after the occurrence of the indicator earthquake with $M \geq M_h > \bar{M}_{\max}$. It is the indicator earthquakes that lead to appearance of dissipative structures and non-equilibrium states in SS at the macroscopic level. Processes in dissipative structures are controlled by power law of entropy production (Akopian & Kocharian 2013) in the magnitude range $M_h \leq M < M_{th}$.

2.4 Dissipation function and seismic time

The change in SS state under the influence of external forces is accompanied by energy dissipation. Let us now consider SS dissipative structures in terms of entropy. Entropy production in the entire system volume per time unit will be called dissipation function

$$\tilde{Q}(t) = \frac{d_i W}{dt} = \frac{E_c(t)}{S(t) \ln 10}, \quad \tilde{Q} = Q \ln 10, \quad (24)$$

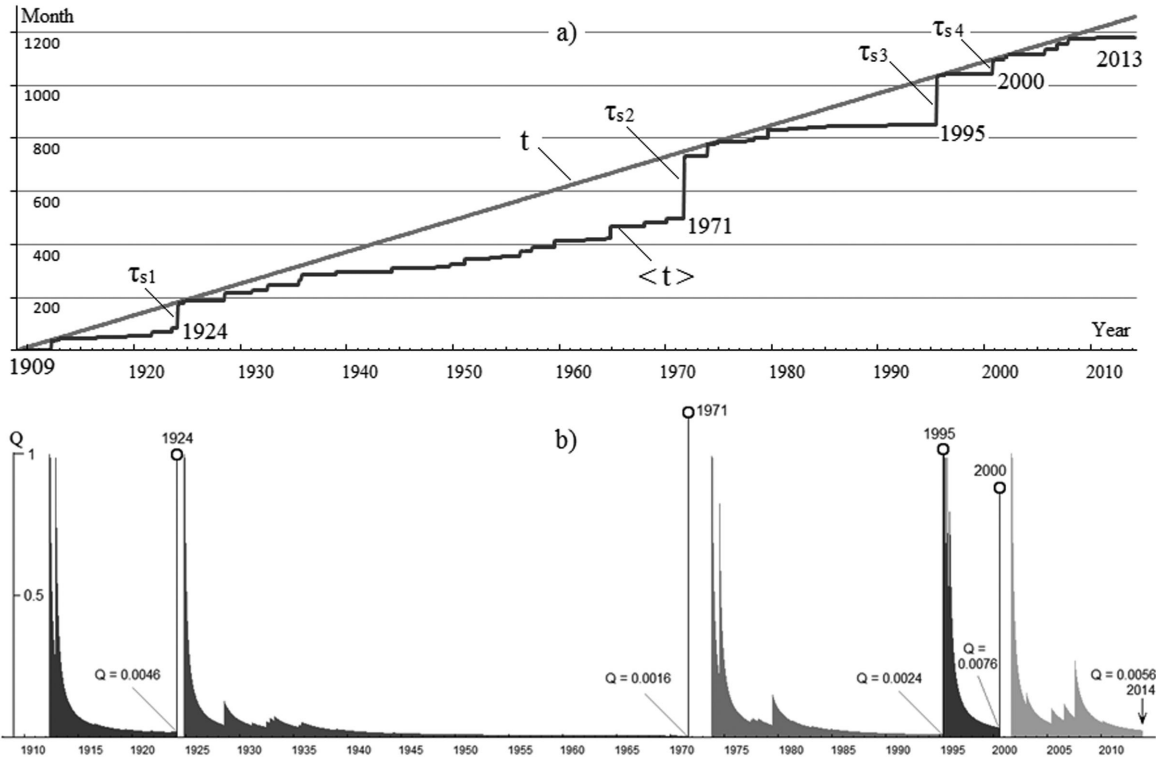


Figure 11. The Sakhalin SS. (a) Time course since 1909 (straight line, the vertical scale it is squeezed) and the internal seismic time (stepwise curve). (b) The dissipative function in seismic cycles.

where \tilde{Q} is the normalized dissipative function $0 \leq \tilde{Q} \leq 1$. The dissipative function Q has the dimension s^{-1} . Here, in contrast to thermodynamics of open dissipative systems (Prigogine 1980), we define the dissipation function not for a volume unit, but for the entire SS volume. If $\tilde{Q} = 0$ or 1 and does not change with time, the state is either equilibrium or stationary equilibrium and the entropy production equals zero. As shown above, the equilibrium state emerges after a strong earthquake (including aftershocks) and remains until the first non-equilibrium earthquake (Fig. 10). At the start of trajectory, $\tilde{Q} = 1$ and then decreases in accord with (24). Using (3), formula (24) in the seismic cycle can be written in the following form:

$$\tilde{Q}(t) = \frac{d_i W}{dt} = \frac{d_i W}{dT} = \frac{1}{(T - \langle T \rangle) \ln 10};$$

$$\langle T \rangle = \frac{\sum_{i=1}^{\tilde{N}(T)} E_i T_i}{\sum_{i=1}^{\tilde{N}(T)} E_i}, \quad (25)$$

where $\langle T \rangle$ is the average ‘seismic time’ (selective average) in the seismic cycle for a set of random discrete times T_i of the indicator earthquakes with energy E_i , $\tilde{N}(T)$ is the number of all indicator earthquakes at time T , counted within the seismic cycle using a regular clock. It will be recalled that the time on a regular clock related to the time in the j seismic cycle by $t = t_{j-1} + T$. The average ‘seismic time’ is defined as $\langle t \rangle = t_{j-1} + \langle T \rangle$. The average ‘seismic time’ $\langle t \rangle$ runs slowly and periodically falls behind the current time t . The ‘seismic time’ helps describe an average ‘age’ of every single dynamical state of SS with all internal communications. The concept of internal time was introduced by I. Prigogine who considered biological time as internal time of the human and assumed that ‘the internal time significantly differs from the external time counted on a wristwatch, it corresponds rather to the age of a human’

(Prigogine 1980). The concept of internal time is close to the concept ‘chronogeography’ (Parks & Thrift 1980). Emergence of internal time is a result of time asymmetry and takes place only for unstable open dynamical systems. Eq. (25) determines the average seismic time of relaxation during a seismic cycle (relaxation means return to the equilibrium state), $\tau = T - \langle T \rangle$, $\tau \geq 0$; note that the average relaxation time determines the order of seismic cycle duration. At the end of seismic cycles, the internal time strongly runs behind the dynamical one; then a strong earthquake in a short-term interval ($\delta t = 1$) compensates a time lag $\tau_s \cong \tau$ and the internal time becomes fitting the dynamical one

$$\tau_s = \langle T_s \rangle - \langle T \rangle, \quad \langle T_s \rangle = \frac{\sum_{i=1}^{\tilde{N}(T_s)} E_i T_i + T_s E_s}{\sum_{i=1}^{\tilde{N}(T_s)} E_i + E_s}, \quad (26)$$

where T_s and E_s are the time and the energy of a strong earthquake, respectively. The value τ_s is the relaxation time of the transition from an unstable state with cumulative energy E_c to the equilibrium state with energy $E_c + E_s$ by means of a strong earthquake. In seismic cycles, the internal time slows down because the seismic time stops (time becomes ‘incompressible’) within time intervals between indicator earthquakes (T_i and T_{i+1}), and only indicator earthquakes move time forward. Once the lag from the real time attains a critical value, j th strong earthquake of ensemble at the end of a seismic cycle compensates this lag τ_{sj} . An example of a seismic time stop is Mars and other planets where there is no seismic activity.

Fig. 11(a) shows the regular time course and the internal seismic time for the Sakhalin SS. These parameters, as well as relaxation and compensation times for strong earthquakes of Sakhalin SS since 1909, are given in Table 2. As is seen, strong earthquakes periodically restore the dynamical time course. It has been shown

Table 2. Parameters of strong earthquakes for the Sakhalin SS. Here, Q is the dissipative function; T and $\langle T \rangle$ are the normal and internal time, respectively, in months; τ is the relaxation time; τ_s is the time compensated by a strong earthquake; T_c° and T_e° (normalized by $\times 10^{-13}$) are the ‘seismic temperature’ and ‘external temperature’ respectively; and ΔT_s° is the compensation of the ‘seismic temperature’.

Year	Q	T	$\langle T \rangle$	τ	τ_s	T_c°	T_e°	ΔT_s°
1924	0.0046	181	87	94	91	8.04	9.86	1.82 (18 per cent)
1971	0.0016	569	317	252	235	70.33	74.01	3.68 (5 per cent)
1995	0.0024	283	101	182	173	30.08	32.93	2.85 (9 per cent)
2000	0.0076	62	6	56	53	19.27	24.31	5.04 (21 per cent)
2013	0.0057	160	83	77	—	36.02	—	—

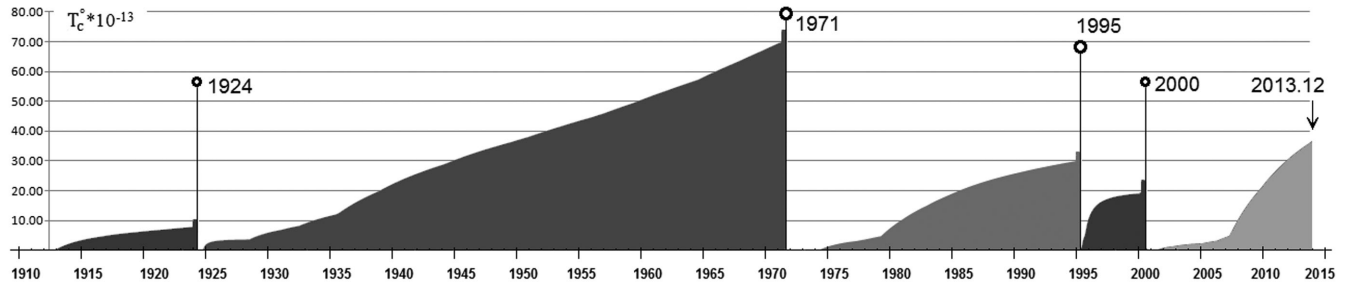


Figure 12. ‘Seismic temperature’ during seismic cycles of the Sakhalin SS.

in Akopian & Kocharian (2013) that SS state during a seismic cycle goes to the power law. Introducing (9) into (24) we obtain the dissipative function limit

$$\tilde{Q} = \beta(S)^{\alpha-1}. \quad (27)$$

The derivative of dissipation function (24) is negative

$$\frac{d\tilde{Q}}{dt} = -\frac{E_c^2(t)}{S^2(t)}, \quad (28)$$

therefore the dissipation function generally decreases with time, but in moments of indicator earthquakes it grows stepwise. This behavior can be seen in Fig. 11(b) where the dissipation function (the rate of seismic entropy production) during the seismic cycles of the Sakhalin SS is shown. By the end of each seismic cycle, the dissipation function goes to minimum, and when indicator earthquakes cannot provide the internal production of entropy for the equilibrium state to be attained, a strong earthquake occurs restoring the balance in the system. Critical values of the dissipative function Q for seismic cycles of the Sakhalin SS are given in Table 2.

By analogy to thermodynamics (Landau & Lifshits 1980; Pathria 2005) and with the use of formulas (3)–(6), we can introduce the concept of ‘seismic temperature’ T_c° for the entire SS volume:

$$T_c^\circ = \left(\frac{dW}{dE_c} \right)^{-1} = \frac{S \ln 10}{T}. \quad (29)$$

Eq. (29) shows that the ‘seismic temperature’ depends on the S/T rate and has energy dimension. Fig. 12 shows the normalized ($T_c^\circ \times 10^{-13}$) graph of the ‘seismic temperature’ during seismic cycles of the Sakhalin SS. Immediately ahead of strong earthquakes, the difference between the ‘temperatures’ of system T_c° and environments T_e° attains the critical value, $-\Delta T_s^\circ = T_c^\circ - T_e^\circ$. Strong earthquakes at the end of seismic cycle increase the system ‘temperature’ stepwise by the value of ΔT_s° and equalize it with the environment ‘temperature’ (Table 2). The system attains to a temporary equilibrium state. Using the concept of ‘seismic temperature’, it is possible to develop the formalism of physics of non-equilibrium states and the theory of dynamical systems applied to seismicity.

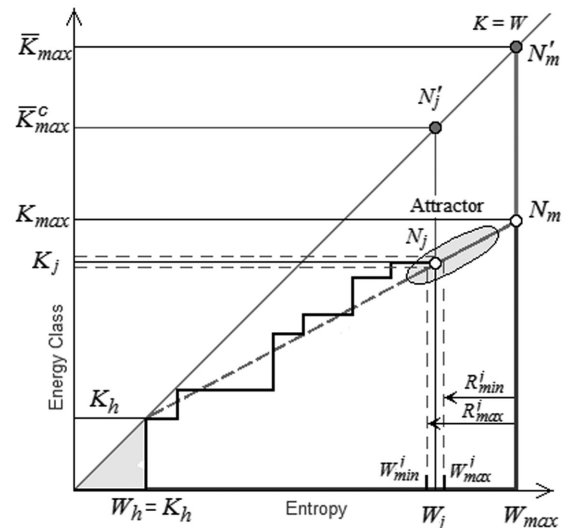


Figure 13. The scheme of coordinates transformation (30) on trajectory diagram. The shown are stepwise trajectory, local instability point N_j of attractor and the respective equilibrium point N'_j on the diagonal. The maximum point N_m and its equilibrium position N'_m are shown right of attractor for transformation. Other notations are in the text.

3 PHASE AND ENERGY DIAGRAMS

3.1 Phase diagrams and entropy funnels

The preparation of a strong earthquake in ensemble can be illustrated using phase diagrams (Glass & Mackey 1988; Nicolis & Prigogine 1989; Akopian 1995b, 2013b). Since the crust has finite limit load strength, entropy of SS has the upper threshold value W_{\max} which is attained in finite time. For each SS, it is possible to choose on the trajectory diagram any point N_m to right of the attractor, where the entropy value $W_{\max} \geq \max\{W_j\}$ (Fig. 13), and to perform coordinate transformation. Let us introduce polar coordinates (R, ϕ) (Akopian

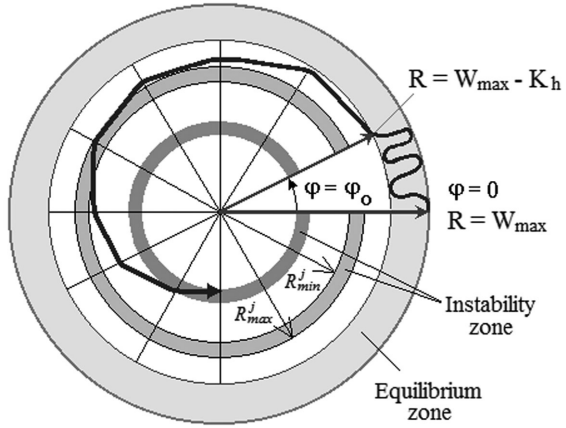


Figure 14. The schematic view of a phase diagram. Concentric dark grey circles are the entropy instability zones for system's elements within attractor. See explanations in the text.

1995b) instead of the entropy and the time in seismic cycle

$$\begin{cases} \phi = T\phi_0 \\ R(T) = W_{\max} - W(T), \text{ at } K_h \leq W \leq W_{\max}, \end{cases} \quad (30)$$

where $\phi_0 = 2\pi/\delta t$ is the angular time step; $K_h = b/(1-a)$ is the energy class of the weakest indicator earthquakes, from which the trajectory starts (Akopian & Kocharian 2013). Fig. 14 gives a schematic representation of the phase diagram. At the beginning of each seismic cycle and in the range $0 \leq W < K_h$, the system is in equilibrium state. In Fig. 14 this state corresponds to the outer shaded annular zone $(W_{\max} - K_h) < R < W_{\max}$. This zone includes noise, microseismicity, aftershocks of the previous strong earthquake.

For each local instability point N_j of the attractor (Fig. 13), let us introduce the pair of threshold parameters on entropy $W_{\min}^j \leq W_j \leq W_{\max}^j$, where $W_{\max}^j - W_{\min}^j = 2\Delta W$ (ΔW is the entropy accuracy). On the phase diagram we define two circles with radii R_{\max}^j and R_{\min}^j (Fig. 14)

$$R_{\max}^j = W_{\max} - W_{\min}^j, \quad R_{\min}^j = W_{\max} - W_{\max}^j. \quad (31)$$

The approach of the trajectory to the attractor in Fig. 13 corresponds to that of R in Fig. 14 on the spiral trajectory to zero, $R(T \rightarrow \infty) \rightarrow 0$. The spiral trajectory will intersect circles (31), at

that. When $R(T)$ falls between the critical circles (31), the respective element of the attractor can transit to an unstable state in a limited time interval if the parameter K_j satisfies the condition (is near the point N_j)

$$K_{\min}^j \leq K_j \leq K_{\max}^j. \quad (32)$$

During time periods when the spiral simultaneously satisfies the conditions (31) and (32), the system will transit to unstable state and a strong earthquake can occur in the respective element of the SS (or fault segment), making the system state correspond to the equilibrium point N'_j (Fig. 13). The way how it happens will be discussed in the next section. The phase diagram illustrates the preparation of each strong earthquake in an ensemble through the spiral trajectory that runs around the limit structural centre of stability. These trajectories, passing through 'holes' in the annular zones, restore the structural stability of the system. For a spiral trajectory, the rate of coordinates R and ϕ at any point of phase space (R, ϕ) can be determined by the following equation system

$$\begin{cases} \frac{d\phi}{dt} = \phi_0 \\ \frac{dR}{dt} = \frac{-dW}{dt} = \frac{-E_c}{S \ln 10} < 0, \end{cases} \quad (33)$$

where ϕ_0 is the constant rate of increase in the angular coordinate ϕ serving as a time counter. The rate of change for radial parameter R depends on the ratio between the cumulative energy E_c and the parameter of state number S . The cumulative energy of indicator earthquakes characterizes the ability of the SS medium to react and adjust the system to external effects, but when the medium loses this resource, a strong earthquake occurs. Since dR/dt is negative, $R(t) \rightarrow 0$ at $t \rightarrow \infty$.

Fig. 15(a) exemplifies the phase diagram of the Neftegorsk earthquake (Sakhalin SS). The maximal entropy value is $W_{\max} = 19.0$, while the lower threshold of indicator earthquake is $K_h = 13$, and the angular step is $\phi_0 = 2^\circ$ (1 month). Annular structures of instability are constructed on the basis of the power law and the parameters of local zones A, B, D, C of the attractor that includes the points of an ensemble of strong earthquakes (Appendix A). The earthquake preparation period was $T_m = 283$ months, and hazard had emerged since 1994 (17 months \sim 6 per cent of the total time of preparation). Fig. 15(b) shows the variations in rate of change for dR/dt and the indicator earthquakes (above)

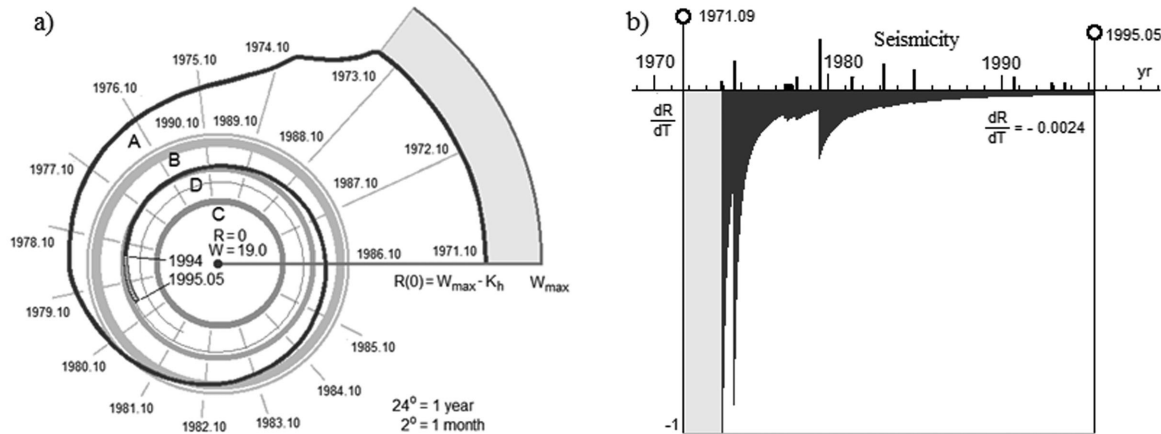


Figure 15. Preparation of the Neftegorsk earthquake (1995 September 9) in the Sakhalin SS. (a) Phase diagram (spiral trajectory); (b) rate the spiral trajectory approach to the diagram centre. The instability zones A, B, C and D on the map are shown on the Fig. A1(c) in Appendix A.

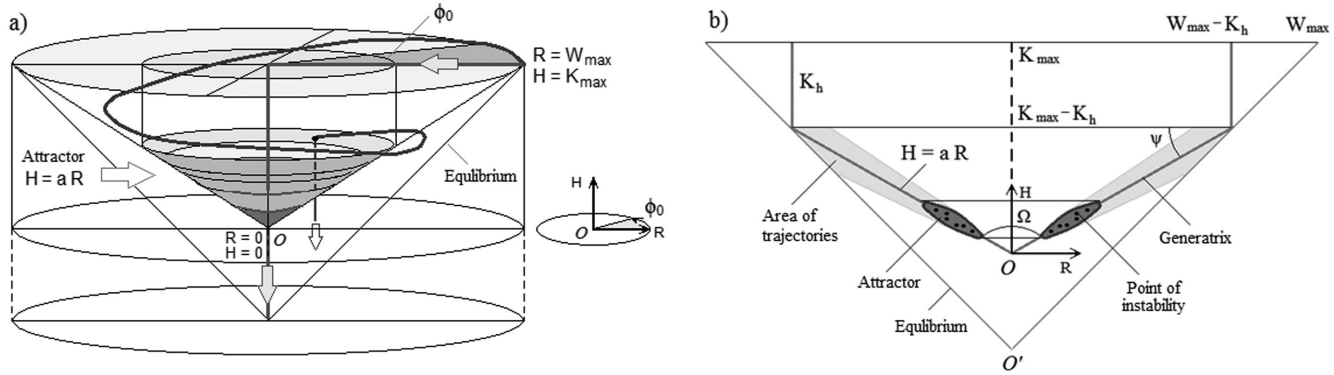


Figure 16. (a) A 3-D view of the phase diagram in the space of time, entropy and energy coordinates. The shaded surface of the cone is a spatial attractor with generatrix $H = aR$. The spiral trajectory is drawn into the funnel and ends in the ‘holes’ within annular zones of the funnel. (b) Vertical cross-section on the plane $\{R, H\}$. Points show the section of the attractor, and the darkened zone is that of spiral trajectories. Ω is the vertex angle of the attractor cone. Cone with vertex O' , height W_{\max} and diagonal generatrix is an equilibrium one.

during the Neftegorsk earthquake seismic cycle. It is seen that in the moments of indicator earthquakes the rate of the spiral trajectory approach to the centre (in absolute value) abruptly increases. For the last months prior to the earthquake, the rate stopped growing and its value just before the earthquake $dR/dt = -0.0024$. The phase diagrams for the strong earthquakes in the SSs of Armenian Upland, Italy and Central California are given in (Akopian 2013b).

Analogous to ‘potential form’ of the equation from the catastrophe theory (Thom 1975; Prigogine 1980; Arnold 1984), transforming the rate of entropy (33), the function R can be considered as any potential function (whose derivative is less than zero) of stress-strain state of the entire SS volume. This function within annular zones of the phase diagram forms group of ‘holes’ (critical points) of strong earthquakes restoring stability in the system. Thom (1975) called these points ‘catastrophe sets’.

For the 3-D representation of the potential function describing a spiral trajectory in a virtual space, let us add the transformation of cumulative energy class into (30)

$$\begin{cases} \phi = T\phi_0 \\ R(T) = W_{\max} - W(T) \\ H(T) = K_{\max} - K(T). \end{cases} \quad (34)$$

The system (34) is defined in the non-equilibrium area

$$0 \leq R \leq (W_{\max} - K_h), \quad 0 \leq H \leq (H_{\max} - K_h). \quad (35)$$

The SS state in a phase space is defined by a point having three coordinates (ϕ, R, H) (Fig. 16). To remind, we consider an unusual space with time, entropy and energy coordinates. The origin of coordinates O in Fig. 16(a) corresponds to the point N_m in Fig. 13, while the origin in Fig. 13 corresponds to the point with coordinates $(0, W_{\max}, K_{\max})$. Let us show that the transformation (34) can represent a dynamical structure of each system in terms of such an unusual space at the macroscopic level in the form of a conical funnel (spatial attractor) having finite depth K_{\max} and surface annular zones of instability. The generatrix of ruled surface of this conical funnel (Fig. 16a) is described by line $H = aR$. The power law (9) on the plane $\{K, W\}$ is described by a linear equation (Akopian & Kocharian 2013)

$$K = aW + b. \quad (36)$$

Introducing (36) into (34), we obtain the following system of equations for the spatial attractor in coordinates (ϕ, R, H) :

$$\begin{cases} \phi = T\phi_0 \\ H(T) = aR(T). \end{cases} \quad (37)$$

Dynamical processes are controlled by medium parameters a and K_h . The value of constant a for real SS ($0.35 < a < 0.82$) corresponds to the angle ψ ($\operatorname{tg}\psi = a$) ranging from 20 to 40 degrees. Then the angle at vertex of attractor cone $\Omega = 2 * (90 - \psi)$ will be 120–140 degrees. The more SS size and threshold magnitude M_{th} are, the deeper attractor cone is located (bigger values of K_h in Fig. 16b) and the bigger the cone angle Ω is.

The preparation of every strong earthquake in an ensemble in Fig. 16 will be displayed by a spatial spiral trajectory (34) that eventually collapses, crosses this structural funnel (truncated cone is a spatial attractor) and ends in the form of seismic catastrophe at a certain spatial point on the surface of truncated cone (37). The upper and lower radii of the truncated cone in Figs 16(a) and (b) equal $\max\{R_{\max}^j\}$ and $\min\{R_{\min}^j\}$, respectively, (31). The final point of earthquake implementation is the cone vertex O ($R = 0, H = 0$). The full equilibrium condition of system for vertex O is the O' with coordinates $(R = 0, H = -W_{\max} + K_{\max})$. Cone surface for real SS (‘relief’) is actually not always smooth and can have roughnesses (tuberous) for complex systems. These roughnesses lead to bifurcations (Haken 1978; Prigogine 1980) that will be considered below through the examples of real systems. Appendix B provides the examples of entropy funnels for the Kamchatka, Central Kuriles, Hokkaido and Sakhalin SSs.

Representation of instability preparation and attractor in the form of a spatial funnel may be significant for the visualization of dynamical instability processes and for non-physical systems. The pattern of the virtual phase space with entropy, energy and time (R, H, ϕ) coordinates represents the dynamical processes and emerging instabilities within dissipative systems in a visually convenient form. It is worth noting that time is one of the three spatial parameters and, at such a view, an equilibrium state of the system (noise, microseismicity) will be on the plane, beyond the funnel.

Macroscopic processes in dissipative structures of an open system periodically lead to the curvature of this surface and the formation of structural funnels (the system becomes 3-D), where eventually spiral trajectories emerge. It is possible to draw an analogy to black holes in the Universe (Hawking 1974; Maldacena 2002). A black hole bends space and distorts (slows down) time current. Analogous

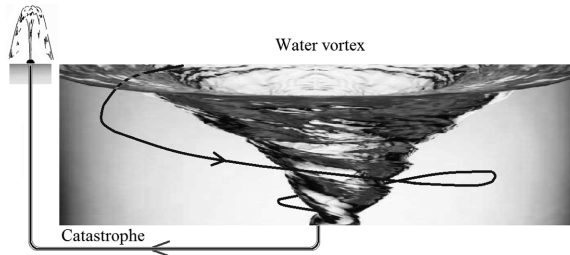


Figure 17. Vortex with a turbulent surface to where small grains of sand (the suspended particles) are drawn by spiral trajectory and then fall into the funnel opening. A fountain schematically illustrates an earthquake as an instant release of particles from the funnel through capillary tube.

to black holes, it is impossible to return from these funnels if the threshold value K_h is attained. Equilibrium state is restored through seismic catastrophes, by releasing of large amounts of elastic and inelastic energies in short time intervals of about $10^{-7} - 10^{-9}$ (of the whole time necessary for drawing into the funnel). It occurs when the spiral trajectory falls at the ‘hole’ on the surface of equilibrium cone (Fig. 16).

There is some similarity between the resulted pattern and the effect of a vortex in a liquid (gravitational-temporal funnel; Fig. 17). The conical surface of vortex is a complex rotation attractor that draws floating suspended particles moving in liquid along spiral trajectories. Return to an equilibrium state (on the undisturbed liquid surface) from such a vortex is impossible without the ‘catastrophe’. The ‘catastrophe’ is schematically shown in Fig. 17 as an instant removal from the vortex through a fountain, but it is a transition to a slightly different equilibrium medium of the same system.

In fact, an ‘entropy’ funnel of SS is built; certain amount of seismic informational entropy in the form of a spiral trajectory is drawn into this funnel and the respective energy ‘catastrophe’ occurs. It is significant that the initial cause of the ‘entropy’ funnel (attraction force) appearance is not an internal force, but the energy from beyond the open system and specific interaction between the system structure and the environment (Section 2.2). Within the SS, under pressure setting, the attraction force is information entropy that controls the total released seismic energy in the system on the basis of the power law (Akopian & Kocharian 2013). This approach makes possible to obtain a 3-D graphical representation (visualization) of the dynamical behaviour of the ‘black box’, described in Section 2.1 (at the lack of information about stress-strain conditions of the environment) based on seismic pulses travelled from the environment and recorded on the surface. An opportunity emerges to implement a computer visualization of the invisible processes leading to extreme situations in both physical and virtual objects, if an array of reliably recorded informative data on an object is available.

3.2 Long- and short-term scales for an ensemble of strong earthquakes

To describe a SS, analogous to open dissipative SSs (Haken 1978; Nicolis & Prigogine 1989; Akopian 1998), two timescales, ‘slow’ T and ‘fast’ ΔT , should be considered. On ‘slow’ timescale, seismic processes lead to emergence of a chaotic state, then the period of cooperation between indicator earthquakes starts for a system and instability development begins. The period of cooperation is characteristic only for ensembles of strong earthquakes. On ‘fast’ timescale, an ordered state of the system is restored by a strong earthquake. The fast timescale is determined by the faulting time τ_s in the source of a strong earthquake and by aftershocks processes.

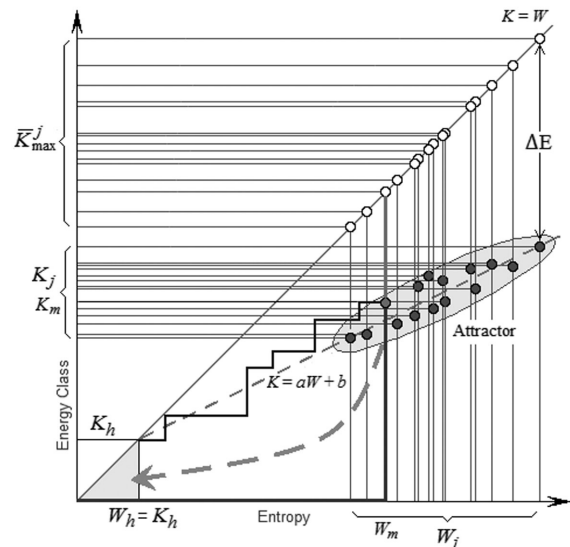


Figure 18. Instability points for an ensemble of strong earthquakes in the attractor and the respective equilibrium points of the diagonal line after energy release ΔE . The current trajectory for the critical point $\{W_m, K_m\}$ of attractor and its return (thick line) from the diagonal line to the origin of coordinates.

Since the release of main seismic energy takes place during the main shock ($\tau_s \leq 60$ s), then nearly always we have $\tau_s \ll \Delta T \ll T$. For example, at the time step $\Delta T = 1$ month, $\tau_s = 4.5 \times 10^{-4} \Delta T$. A strong earthquake occurred in the fast time interval ΔT transfers the SS from points of attractor instability to the equilibrium state.

Let us consider the seismic energy balance of the SS when this transition occur. As shown in Fig. 13, it is possible to find the respective point on a diagonal equilibrium N'_j , for every point of attractor instability N_j ; at any of these points, $\bar{K}_{\max} = \bar{W}_{\max} = W_e(T_m + \Delta T)$, where W_e is the total entropy at the end of a seismic cycle. Trajectory can instantly reach the equilibrium point N'_j through only one hypothetical equilibrium earthquake with the maximal energy of $\bar{E}_{\max} = 10^{\bar{W}_{\max}}$ (see Section 2.2). Such a trajectory for the point N'_m is denoted with a thick line in Fig. 13. The total energy transferred from beyond the SS during $T_m + \Delta T$ will be assumed to be \bar{E}_{\max} energy of a hypothetical earthquake. It means the entropy is a measure of the flow of the external energy in a SS; this is released in focal zones of earthquakes and is consumed for inelastic processes in the system volume. With this in mind, the formula (13) for inflow (negative) and outflow of entropy on ‘fast’ timescale (at the end of every seismic cycle) can be written as follows:

$$dW = d_e W + d_i W = -W_e(T + \Delta T) + \frac{E_c + \Delta E}{S \ln 10} \Delta T, \quad (38)$$

where E_c is the total elastic energy in discrete sources of indicator earthquakes; S is the number of states on ‘slow’ timescale before a strong earthquake; ΔE is the energy released on ‘fast’ timescale ΔT and raising the trajectory to the respective equilibrium point of the diagonal line on the trajectory diagram. Fig. 18 schematically shows the mechanism of the trajectory return to the origin of coordinates for an ensemble of strong earthquakes. At points of attractor instability, after an intensive release of elastic and inelastic energy in the source of a strong earthquake, the trajectories fall at the respective equilibrium points of the diagonal line, the system attains equilibrium with the environment and a new trajectory starts at the origin of coordinates. With respect to this, the energy ΔE (lack of energy relative to the equilibrium point of the diagonal line) on

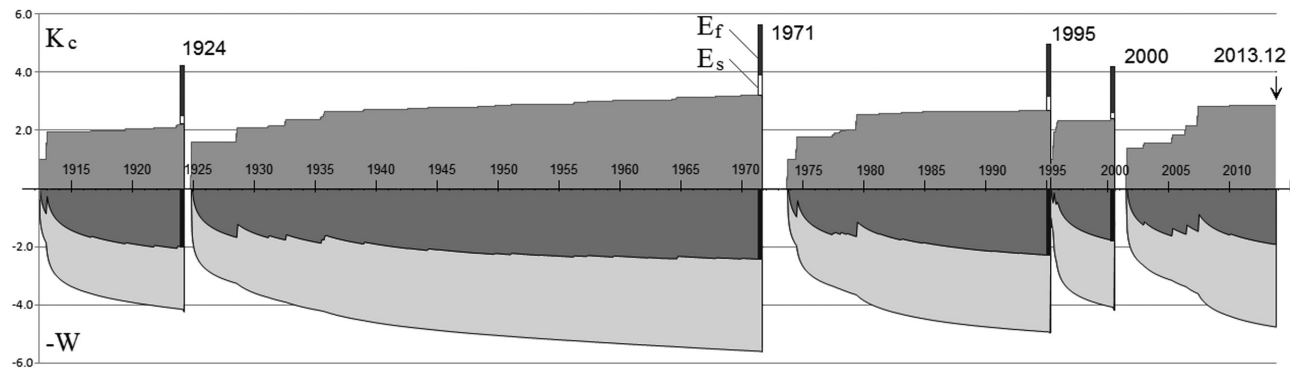


Figure 19. Seismic cycles of the Sakhalin SS. The graph of: cumulative energy class K_c (upper); entropy W – is equal to logarithm of the energy flux in the system (lower) and their sum (middle). The graphs show elastic E_s and inelastic energies E_f of the strong earthquakes in 1924, 1971, 1995 and 2000, which restored the lacked energy state at the ends of seismic cycles.

'fast' timescale can be written in the following form:

$$\Delta E = (E_s + E_f), \quad E_f = E_{fs} + \sum E_{fi}, \quad (39)$$

where E_s is the elastic energy release from a strong earthquake; E_f is the total inelastic energy (E_{fs} is the inelastic energy in the source of a strong earthquake and E_{fi} is that of the i th indicator earthquake). Introducing (39) into (38) and using expansion $W_e(T + \Delta T) \cong W(T) + (dW/dT)\Delta T$, we can write the equilibrium condition at the end of every seismic cycle after a strong earthquake as follows:

$$-W(T) - \frac{E_c + E_s}{S \ln 10} \Delta T + \frac{E_c + E_s + E_f}{S \ln 10} \Delta T = 0, \quad (40)$$

Therefore, at $\Delta T = 1$, we can find inelastic energy

$$E_f = W S \ln 10. \quad (41)$$

This formula was obtained earlier (Akopian 1995c, 2013b). Thus, the entropy of the statistical equilibrium ensemble (Nicolis 1986) of strong earthquakes helps calculate the value of the total inelastic seismic energy during seismic cycles.

Below, the balance of the energy supplied and released during seismic cycles will be illustrated as exemplified by strong earthquakes of the Sakhalin SS. Upper part of Fig. 19 shows the graph of cumulative energy class $K_c = \log E_c$ during seismic cycles of the Sakhalin SS (scale is increased by two orders); the lower part exhibits the graph of logarithm of the energy flux in the system, $K_{es} = W$. The middle graph in Fig. 19 is the total non-compensated energy $K_k = W + K_c < 0$ (the difference between the inflow and the total release of elastic seismic energy radiation in the sources of all indicator earthquakes). The value K_k is negative and decreases with time (while increases in absolute value), surging in the moments of indicator earthquakes. These surges mean that indicator earthquakes tend to transfer the SS to equilibrium with the environment. Once K_k reaches the critical value in a short-term interval ΔT , a strong earthquake restores the energy balance in accord with (38)–(41).

3.3 Energy diagram: the law of seismic entropy production on fast scale

Now let us discuss one of the fundamental problems of medium dynamics and seismology: how energy (magnitude) of an expected strong earthquake can be predicted. On the basis of experimental studies of such seismoactive regions as Tauro-Caucasus, Italy, California, Iran, Sakhalin and Hokkaido-Kuriles-Kamchatka

(Akopian 1998, 2013a,b; Akopian & Rogozhin 2013), a seismic regularity was revealed; this regularity controls the elastic energy of an ensemble of strong earthquakes, depending on seismic entropy, in so called homogeneous seismotectonic zones (HSZ). HSZ are domains within the SS incorporating the groups of strong earthquakes based on some characteristics. They can be grouped in terms of focal mechanisms, coincidence to faults, spatial arrangement in the SS volume, trajectory configuration, etc. The criteria for selection of HSZ are the regularities of instability points' arrangement in the attractor on the trajectory diagram and the radiation energy (magnitude) of strong earthquakes of the equilibrium ensemble. For HSZ, the energy released by strong earthquakes on 'fast' timescale ΔT follows the law (Akopian 1995a)

$$E_s = 10^{a_s W + b_s} = \beta_s S^{a_s} \quad (\beta_s = 10^{b_s}), \quad (42)$$

where a_s and b_s are the constants; E_s is the seismic energy released by a strong earthquake in HSZ. Formula (42) can be written in the linear form

$$K_s = a_s W + b_s, \quad (W_{\min} < W < W_{\max}) \quad (43)$$

where $K_s = \log E_s$. Constants a_s and b_s are defined by the regression method (Rade & Westergren 2004) on the basis of entropy and energy class of strong earthquakes $\{W_j, K_{sj}\}$ for finished seismic cycles j . The diagram of macroscopic behaviour of the SS on 'fast' timescale and on the plane $\{W, K_s\}$ was called an energy diagram (Akopian 1998). The energy diagram helps predict energy (magnitude) of an expected strong earthquake (see Appendix A). In contrast to the constant a of the power law (9) on 'slow' timescale on the trajectory diagram, the constant a_s may be negative. In particular, the zones with negative a_s were found in Italy and Central California (Akopian 1998, 2013b), and also in Japan (Akopian 2013a). For HSZ with negative a_s , the expected magnitude of a strong earthquake decreases as entropy grows. It takes place in fault zones where creep processes, high thermal emissions and plastic deformations dominate. Usually strong earthquakes in such HSZ have a normal focal mechanism.

The energy diagram of the Sakhalin SS is exhibited in Fig. 20(a). After finishing the five seismic cycles, the strong earthquakes of an ensemble in this system form one HSZ. Using the data from columns K_s and W_j of the Table A1 (Appendix A), let us find the linear equations of regression (43), before and after the 2000 earthquake

$$K_s = 0.526W + 7.000, \quad K_s = 0.456W + 8.208, \quad W > 15.50. \quad (44)$$

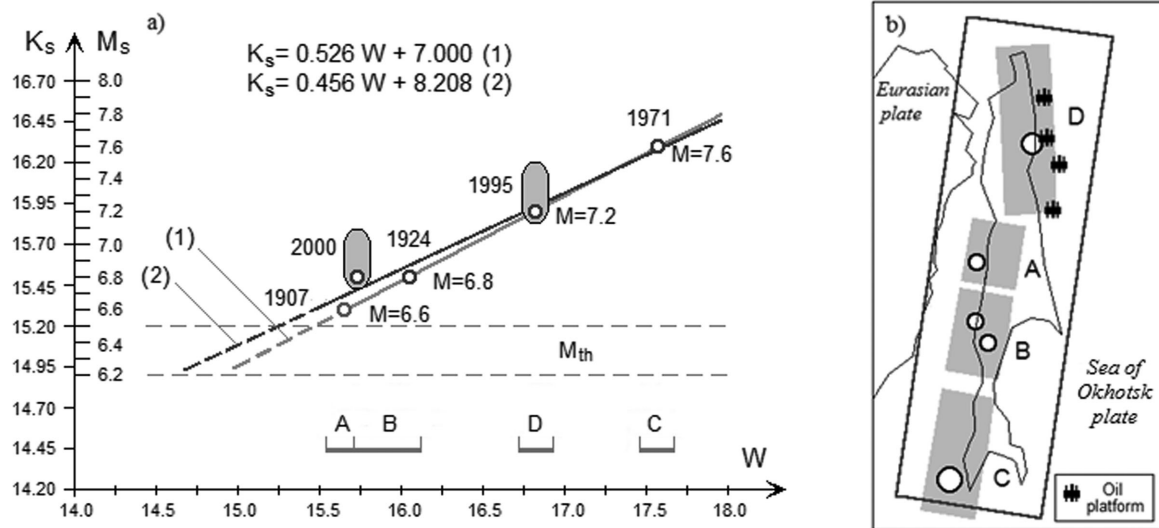


Figure 20. Sakhalin SS. (a) Energy diagram: (1) until 2000 as constructed in (Akopian 1998) and (2) after 2000 based on four points. The shaded zones denote scatter of magnitudes. (b) Source zones A, B, C and D of five strong earthquakes and oil platforms. Entropy-based instability area corresponding to these zones is shown on the energy diagram. Open circles denote instability points and the epicentres of strong earthquakes with $M > 6.2$.

These linear equations of regression, are shown in Fig. 20(a) (eqs 1 and 2). Average magnitudes of strong earthquakes on the diagram correspond to the energy of the earthquakes prepared by the real geological structure of SS for many decades. The traditional magnitude found from the records of seismic waves may be affected by variations in fluids of the medium, artificial and technogenic factors in the focal zone for shorter time intervals; all these factors can both increase and reduce energy of a prepared earthquake. A comparison between the predicted magnitudes of strong earthquakes, found by the method of seismic entropy on the energy diagram, and the traditional magnitudes found from the data of seismic networks reveals the fluid and technogenic components in earthquake preparation.

So, instrumental magnitudes of the 1995 Neftegorsk and the 2000 Uglegorsk earthquakes in the Sakhalin SS (defined by different networks) had some scatters (Fig. 20a). As can be seen that the lower values of magnitudes of these earthquakes better fit the eqs (1) and (2). It means that the magnitudes of natural tectonic earthquakes were amplified during the seismic cycles of these events. This could be the effect of technological developments as a result of which there was a variations in content of natural hydrocarbon fluids (Akopian & Popov 2010; Akopian 2014). Indeed, the oil and gas production in the shelf zone of northern Sakhalin (Fig. 20b) since 1971 coincided with the beginning of a cycle of the Neftegorsk earthquake preparation. It could affect the natural processes and amplify the resulted magnitude of the Neftegorsk earthquake. Despite the source of the Uglegorsk earthquake was located in the central Sakhalin (Fig. 20b), the SS on the whole is responsible for its preparation. The technogenic changes in the system volume could violate the natural course of seismic processes and accelerate preparation of the Uglegorsk earthquake. If it occurred few years later, its magnitude would better fit the value expected from the energy diagram. Despite the fact that the oil and gas extraction was carried out far from the focal zone of the Uglegorsk earthquake (northern Sakhalin), these works took place within the Sakhalin SS and might play a role of indicator earthquakes and trigger the earthquake before its ‘natural’ time.

4 ENERGY BALANCE AND DYNAMICAL PROBABILITY IN SEISMIC SYSTEMS

4.1 Efficiency of SSs

In this section, let us give a definition of the efficiency factor η_{ct} of the SS during the entire seismic cycle in terms of seismic entropy. It can be presented as the ratio between the change of entropy and the total entropy (Akopian 2013b)

$$\eta_{ct}^w = \frac{\Delta W}{W} = \frac{1}{W} \frac{\Delta S}{S \ln 10}. \quad (45)$$

At $S \gg \Delta S$ and using the expansion formula

$$W = \log(S + \Delta S) \cong \log S + \frac{\Delta S}{S \ln 10}, \quad (46)$$

we can transform (45) to

$$\eta_{ct}^w = \frac{\Delta S}{\ln(10)S \log S + \Delta S}. \quad (47)$$

Between successive indicator earthquakes, the value ΔS is constant ($\Delta S = E_c$), while grows stepwise in the moments of indicator earthquakes with energy E_i , $\Delta S = E_c + E_i$. At the end of a seismic cycle, when a strong earthquake occurs, $\Delta S = E_c + E_s$, and the efficiency factor (47) can be written as follows:

$$\eta_{sc}^w = \frac{E_s}{\xi \ln(10)S \log S + E_s}. \quad (48)$$

Here, we introduce the specific energy parameter

$$\xi = \frac{E_s}{E_c + E_s} \quad (49)$$

depending on the ratio between cumulative energy of indicator earthquakes and energy of a strong earthquake, E_c/E_s . If $E_c \ll E_s$, then $\xi = 1$ and if $E_c \cong E_s$, $\xi = 0.5$. At $\xi = 1$, formula (48) describes the SS efficiency in the moment of a strong earthquake occurrence. The parameter ξ (49) is also important for estimating the fraction

of invisible inelastic ('dark') energy (41) released by SS on 'slow' and 'fast' timescales.

The efficiency factor (48) of SS essentially differs from the efficiency of seismic radiation for earthquake sources in seismology (Wiss & Brune 1971; Kasahara 1981). The factor η_{sc}^w characterizes the cumulative irreversible processes related to the work to overcome friction force and heat generation both in the focal zone and the entire SS volume during preparation and implementation of a strong earthquake. For strong earthquakes of the Sakhalin SS, ξ and η_{sc}^w values are given in Table A1 (Appendix A). High ξ values indicate that the major part of inelastic energy (~93–96 per cent) is released by strong earthquakes within seismic cycles, whereas the rest inelastic energy (~7–4 per cent) was done during the preparation of these strong earthquakes. Less than 0.5 per cent of energy was supplied for elastic seismic energy radiation. The same parameters for strong earthquakes of the Armenian Upland and the Japan SS are given in (Akopian 2013a; Akopian & Rogozhin 2013). For the Tohoku earthquake (2011 March 11, $M = 9.0$), $\xi = 0.32$ and $\eta_{sc}^w = 0.01$ per cent in the megasystem of Japan ($M_{th} = 8.4$) and $\xi = 0.88$, $\eta_{sc}^w = 0.48$ per cent in the system of Japan ($M_{th} = 7.8$). For the Van earthquake in the eastern Turkey (2011 October 23, $M = 7.4$), the $\xi = 0.42$ and $\eta_{sc}^w = 0.02$ per cent. Thus, the respective SSs consumed enormous efforts for preparation of these earthquakes.

4.2 Energy balance in sources of strong earthquake

At the end of every seismic cycle, a total energy balance can be written as follows:

$$E_e = E_f + E_c + E_s, \quad (50)$$

where E_e is the energy inflow into the system (1), E_f is the inelastic energy (41), E_s is the energy release from a strong earthquake (42), and E_c is the cumulative energy of indicator earthquakes (3). Tectonic energy is redistributed in the system volume and consumed for irreversible processes and seismic radiation. Inhomogeneities within the system (active and inactive faults) involved into this process contain the contacting fault planes, along which shear destructions can propagate. For a local fault zone that can generate a strong earthquake in the system, the common stick-slip mechanism (Brace & Byerlee 1966; Brace *et al.* 1966; Byerlee 1967; Rice 1980) is assumed. Stick-slip is a non-uniform slide with friction between two contacting blocks, with the main role played by the difference between static and kinematic frictions.

It is assumed after (Scholz 1990) that two surfaces of a fault having the contact area A are mutually coupled by the contacting asperities of the total area $A_r < A$, where A_r is not constant in time (A_r is the real contact area, A is the full area of contacting surfaces in Fig. 21). Let us introduce the parameter $\kappa = (1 - A_r/A)$. At weak contact, $A_r \ll A$ and $\kappa \approx 1$; in contrast, when $A_r \rightarrow A$ and $\kappa = 0$, the fault is locked. Let the SS volume have j inhomogeneities (elements) having contact surfaces of A_{rj} and being able to generate a strong earthquake. At the beginning of a seismic cycle, it is assumed that values of parameter κ_j for these contact surfaces are close to zero. The real contact surfaces of faults $A_{rj}(t)$ depend on time because they will change during trajectory development in an open SS, depending on tectonic situation and external pressure conditions.

If the shear stress on contacting surfaces increases, a slid will begin at an element of SS where the accumulated shear stress exceeds the average static friction stress (Fig. 21)

$$\tau^j = (\mu_s \sigma_n)^j, \quad (51)$$

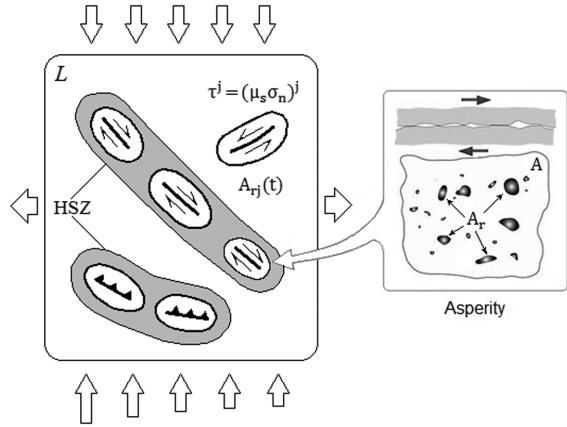


Figure 21. Schematic view of HSZ and local zone of potential rupture and slips. See explanations in the text.

where j is the element number in the system volume, μ_s is the factor of static friction, σ_n is the local normal stress. As is shown by laboratory experiments (Dieterich 1978a,b) the factor of static friction μ_s , as well as a real contacting surface, can change with time. One of the reasons why μ_s can grow is the increase in coupling on contacting surfaces of the j th element of the system due to smoothing of asperities; the opposite pattern can be observed due to brittle destruction of coupled areas and the formation of friction clay. The SS energy balance for the emergence of a strong earthquake in the j th element of the system, can be written as follows:

$$\ln(10)S \log S + \beta_s S^{a_s} = (\mu_s \sigma_n u A_r)^j, \quad (52)$$

where u is the expected slip in the j th element.

Physical processes in heterogeneity zones (on contact surfaces) of the real SS are quite complex, poorly studied and, in fact, cannot be controlled. From a mechanical viewpoint, the problem cannot be solved due to the lack of relevant data on real behaviour of contacting surfaces of faults in large SS volumes. All values of μ_s , σ_n and A_r in the right-hand side of eq. (52) have a common feature: they are time dependent, so instability 'gets matured' with time. The introduction of time-dependent parameter S describing a number of system states helps control these values and define energy balance in the sources of expected strong earthquakes. The element of system and time when there will be a loss of stability (52) are defined on the basis of the trajectory diagram and attractor. For this purpose, a number of the new parameters can be also used; these parameters are introduced in Sections 2.4, 4.1 and in the next section as well.

4.3 Dynamical probability

In Section 2.1, it was noted that the probability distribution of cumulative energy within the seismic cycle (12) coincides with the Poisson distribution for a limited interval $E \in [1, S]$. It means, that (in contrast to the Poisson distribution) the probability distribution $p(E)$ of indicator earthquakes cumulative energy depends on two parameters E and S . The situation is different when not a single seismic cycle is considered, but the set of n of the finished seismic cycles in the SS, forming an ensemble of strong earthquakes. The instability points of the strong earthquakes $\{W_j, K_{cj}\}$ ($j = 1, 2, \dots, n$) fill some local elliptic area near the line (36). The discrete values of the controlling parameters W_j and K_{cj} are considered as a set of two independent tests of the SS. They are filling narrow finite intervals along the axes ($W_{\min} \leq W_j \leq W_{\max}$, $K_{\min} \leq K_j \leq K_{\max}$) on the trajectory diagram (see Fig. 18) and depends from the mean

Table 3. Dynamical probability for the strong earthquakes of the Sakhalin SS.

Place	Year	W_0	σ_W	K_0	σ_K	P_W	P_K	P
Uglegorsk	1924	15.95	0.20	14.19	0.01	—	—	—
Moneron	1971	16.52	0.83	14.54	0.50	~1	~1	~1
Neftegorsk	1995	16.62	0.68	14.57	0.43	0.682	0.606	0.414
Uglegorsk	2000	16.46	0.73	14.47	0.44	0.137	0.124	0.017
	2014	—	—	—	—	0.658	0.830	0.546

values $\langle W \rangle$, $\langle K \rangle$, and the dispersions σ_W^2 , σ_K^2 relative to these average values (Akopian & Kocharian 2013), that is described by a Gaussian distribution. In other words, the Poisson distribution is applicable to indicator earthquakes in a seismic cycle for any limited large interval $E \in [1, S]$, while strong earthquakes of the ensemble are described by the Gaussian distribution in the relatively narrow intervals.

Let we have n ($n \geq 2$) of the finished seismic cycles. For the $n + 1$ incomplete seismic cycle at the current time $T_m = t_m - t_n$ introduce the dynamical (time-dependent) probability of system stability loss. The current parameters of seismic entropy W_m and cumulative energy class K_m , calculated at the time T_m (on the basis of random indicator earthquakes), will be considered as independent random variables. Assume that the system attains the unstable state when both parameters satisfy $W_m \in [W_{\min}, W_{\max}]$ and $K_m \in [K_{\min}, K_{\max}]$. For well-defined systems (usually the systems with $n \geq 10$), these conditions are satisfied. Then the dynamical probability of system stability loss in the system can be determined as the product of the probabilities of finding the parameters W_m and K_m at the respective intervals (Akopian 1995c, 2013b)

$$P(W_m K_m) = P(W_m)P(K_m). \quad (53)$$

Here, probabilities on entropy P_W and on cumulative energy class P_K are determined by formulas of normal distribution (Kolmogorov 1974)

$$P(W_m) = \int_0^{W_m} f(W)dW, \quad (54)$$

$$f(W) = \frac{1}{\sigma_W \sqrt{2\pi}} \exp\{-(W - W_0)^2/(2\sigma_W^2)\}, \quad (55)$$

$$P(K_m) = \int_0^{K_m} f(K)dK, \quad (56)$$

$$f(K) = \frac{1}{\sigma_K \sqrt{2\pi}} \exp\{-(K - K_0)^2/(2\sigma_K^2)\}, \quad (57)$$

where $f(W)$ and $f(K)$ are the Gaussian functions of the probability distribution density, W_0 and K_0 are the expected values of entropy and cumulative energy class, respectively, σ_W and σ_K are the mean square deviations (measures how far data points are spread out), calculated using W_j and K_j ($j = 1, 2, \dots, n$) of previously ended seismic cycles by the formulas:

$$W_0 = 1/n \sum_{j=1}^n W_j, \quad \sigma_W = \left\{ \sum_{j=1}^n (W_j - W_0)/n \right\}^{1/2}, \quad (58)$$

$$K_0 = 1/n \sum_{j=1}^n K_j, \quad \sigma_K = \left\{ \sum_{j=1}^n (K_j - K_0)/n \right\}^{1/2}, \quad (59)$$

Gaussian functions of probability for seismic cycles of the Armenian Upland, NW Iran, Italy and Central California SSs were calculated in (Akopian 2013b). These parameters for seismic cycles of the Sakhalin SS are given in Table 3. If the system is well defined (i.e. there is a large statistics of strong earthquakes), after

each new strong earthquake the mean square deviations decrease. Table 3 shows that the SS Sakhalin refers to poorly defined, since after the last strong earthquake in 2000 the standard deviations have increased slightly.

The probability of entropy can be expressed through the current time T_m passed after the end of the previous cycle (Akopian 1995c)

$$P_W(0 \leq T \leq T_m) = \int_0^{T_m} \Phi_W\{W(T)\}dT, \quad (60)$$

$$\Phi_W = \frac{1}{\sigma_W \sqrt{2\pi}} dW/dT \exp\{-(W - W_0)^2/(2\sigma_W^2)\}, \quad (61)$$

where

$$dW/dT = 1/(S \ln 10) dS/dT, \quad (62)$$

and Φ_W is the lognormal function of probability density distribution, defined by the parameters of normal distribution W_0 and σ_W , and depending on the entropy derivative (\dot{W}) .

The probabilities P , P_W and P_K are the parameters of SS instability monitoring and they have remarkable features. The probability P_K grows stepwise at the time moments of indicator earthquakes, while the probability by entropy P_W grows continuously over time. The local attractor domains characterizing the dynamics of different segments of seismically active faults have different values of probability (not necessarily large) of system stability loss. Let us consider the dynamical probability of the Sakhalin SS in more detail. Fig. 22(a) shows the 3-D surface of the probability P , the arrangement of the seismic attractor and the distribution of strong earthquakes (points of instability) for this system. On the plane $\{W, K\}$, the probability of stability loss is close to zero, while trajectories run beyond the attractor (out of the ‘hill’). The probability value starts to grow when the trajectory approaches the ‘hill’, enters the attractor and tends to 1 at the top of the ‘hill’. Fig. 22(a) shows that the attractor is limited by the areas of greatest curvature of probability isolines. It means that trajectories are attracted to the corner part (to the edge) of the ‘hill’, where the probability P is the highest at each fixed level. Hazard depends on the ratio between two probabilities, P_W and P_K . The highest hazard level will be at $P_W \cong P_K$; that is when the trajectory is within the attractor and very close to the power law (9). Fig. 22(a) shows the last trajectory within an unfinished seismic cycle at the beginning of 2014 (empty circle). Despite the high probability value, $P = 54.62$ per cent, the probability on entropy is less than that on cumulative energy, $P_W < P_K$ (see Table 3); therefore, there is no hazard in the system yet. The stepwise arrow denotes the trajectory progress to the attractor at constant E . The graphs of dynamical probabilities P , P_W and P_K for the Sakhalin SS at the trajectory progress from 2000 to 2014 are given in Fig. 22(b). It shows that, in the case of seismic quiescence in the system, hazard will emerge by 2024, when $P_W \cong P_K$.

The density function of lognormal probability distribution is a basis for earthquake prediction in California (Nishenko & Buland 1987; Page *et al.* 1992). In these works, probabilities were calculated on the basis of long-term rate of potential earthquake

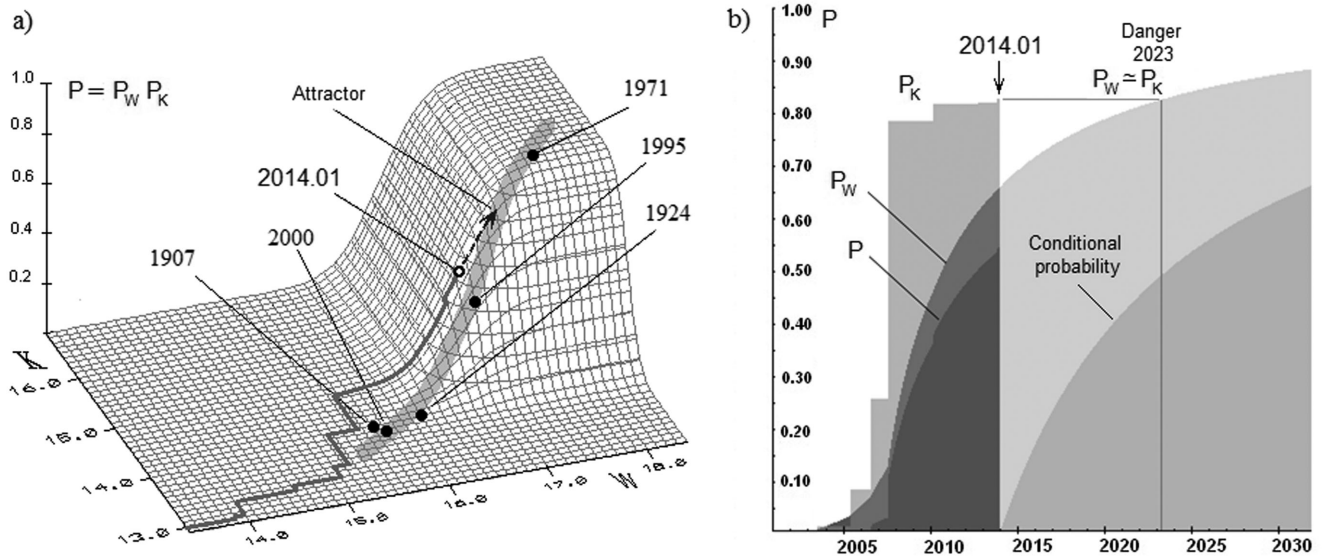


Figure 22. (a) The 3-D view of probability growth on the track diagram (horizontal plane) of Sakhalin SS. Axis W denotes the growth of probability P_W ; axis K , the probability P_K ; vertical axis, the probability P . Increase in probability falls at the area of attractor (along the edge of probability ‘hill’). The shown trajectory (indicated by the stepwise arrow) is for an unfinished cycle and it progresses to the intersect with the attractor. (b) Dynamical probabilities P , P_W , P_K from 2000 to 2014 in the Sakhalin SS. It is shown that $P_W \cong P_K$.

ruptures (above certain threshold magnitude) (Field *et al.* 2009; Field & Page 2011). That approach has no strict mathematical criterion for selecting of both fault segments and threshold magnitudes, so the assessment was made at 30-yr averaging (WGCEP 2003). In our approach, probability is defined for a faults system included in the SS, these probability values are dynamical and they change (grow) in real time (depending on any chosen time step). They are calculated at several hierarchical levels for SS volumes with different threshold magnitudes. If quite a long series of seismic observations is available, then it is possible to calculate the values W_0 , K_0 , σ_W and σ_K by (58), (59), and to find normal distributions (54)–(57) in real time; this can be done after every seismic cycle beginning with the second one.

If there was no earthquake until the current time moment T_m , the probability of stability loss in future, for the period of $T_m \leq T \leq T_i$, can be expressed by the following formula

$$P(T_m \leq T \leq T_i | T > T_m) = P_W P_K, \quad (63)$$

where, in contrast to (41), P_W is the conditional probability of entropy and is found by the formula

$$P_W(T_m \leq T \leq T_i | T > T_m) = \frac{P_W(T_m \leq T \leq T_i)}{1 - P_W(0 \leq T \leq T_m)}, \quad (64)$$

The conditional probability as of 2014 January in the Sakhalin SS is shown in Fig. 22(b).

5 CONCLUSION

SSs are open dissipative systems that exchange energy and entropy with the environment. The earlier introduced parameters of seismic entropy and cumulative energy, as well as the concept of SS and an ensemble of strong earthquakes, permit to apply the knowledge from the modern theory of dynamical complex systems to seismicity. This creates a physical basis for understanding of processes of instability emergence in the geological medium and helps predict the medium behaviour. An opportunity arises to make a new look at seismic pro-

cesses and to reinterpret the seismostatistical information collected over many decades. The proposed approach enables to model and visualize the dynamics of medium behaviour at the lack of necessary information about the internal state of the medium; in addition, a complex problem of a critical behaviour of dissipative structures in discrete volumes of the geological medium can be solved. For this purpose, such parameters as entropy, cumulative energy, ‘seismic temperature’, ‘seismic time’, dissipation function, efficiency of system, inelastic energy and dynamical probability have been introduced; it worth noting that, these parameters can be calculated in real time by mathematical methods and used for monitoring of seismic instability. The Poisson distribution is applicable to indicator earthquakes in the seismic cycle, while the strong earthquakes of an ensemble are described by the Gaussian distribution. For the chosen time step, the asymmetry of indicator earthquakes distribution leads to the appearance of dissipative structures and non-equilibrium SS states at the macroscopic level. There is no criterion of instability in the domain where the GR law is true because, analogous to the Liouville equation in thermodynamics, the GR law does not describe the dynamics of deviation from stable and that of instability emergence. Dissipative processes and energy balance in open SS are controlled by information entropy at stages of a strong earthquake preparation and implementation. Construction of phase diagrams and ‘entropy funnels’ in the virtual space (with time, energy and entropy coordinates) can offer the new opportunities to visualize invisible processes of catastrophes’ preparation and to look at the problem of black holes origin in the Universe from an unordinary, seismological viewpoint.

ACKNOWLEDGEMENTS

The author thanks the anonymous reviewers for thoughtful and constructive comments, and N.N. Astafiev for a careful reading of the manuscript and valuable comments that improved the paper.

REFERENCES

- Akopian, S.Ts., 1995a. Entropy of a seismic system and a new seismic law, *Dokl. Ross. Akad. Nauk*, **340**, 531–535.
- Akopian, S.Ts., 1995b. Seismic entropy monitoring and earthquake prediction problem, *Dokl. Ross. Akad. Nauk*, **341**, 247–250.
- Akopian, S.Ts., 1995c. Probabilistic approach to earthquake prediction problem and seismic system work effectiveness, *Dokl. Ross. Akad. Nauk*, **341**, 682–685.
- Akopian, S.Ts., 1998. Quantitative description of seismic processes based on seismic entropy, *Izv. Ross. Akad. Fiz. Zemli*, **1**, 11–26.
- Akopian, S.Ts., 2007. Dissipative seismic systems, entropy, and possibility of creation the system of ‘seismic weather’ forecast, *Business Glory of Russia, Interdisciplinary Almanac*, III, 42–46.
- Akopian, S.Ts., 2013a. Seismic systems of the Japan, entropy and monitoring of the mega earthquake Tohoku on March 11, 2011, *Probl. Eng. Seismol.*, **40**, 67–90.
- Akopian, S.Ts., 2013b. *Quantitative description of seismic processes in real medium and the algorithm of long-term prediction of large earthquakes: By examples of Armenian Upland, North-Western Iran, Italy, and Central California*, Moscow, Triumph.
- Akopian, S.Ts., 2014. Application of seismic entropy to increase frac efficiency, *ROGTEC*, **38**, 54–61.
- Akopian, S.Ts. & Kocharyan, A.N., 2013. Critical behaviour of seismic systems and dynamics in ensemble of strong earthquakes, *Geophys. J. Int.*, **196**(1) 580–599.
- Akopian, S.Ts. & Popov, E.A., 2010. Monitoring induced seismicity based on seismic entropy method, Abstracts, Induced Seismicity ECGS-FKPE Workshop, 15–17 November, Luxembourg, pp. 3–4.
- Akopian, S.Ts. & Rogozhin, E.A., 2013. Modeling kinematics of the Tauro-Caucasus region and dynamics of strong earthquake preparation with $M \geq 7.1$, *Probl. Eng. Seismol.*, **40**, 5–24.
- Al-Kindy, F.H. & Main, I.G., 2003. Testing self-organized criticality in the crust using entropy: a regionalized study of the CMT global earthquake catalogue, *J. geophys. Res.*, **108**, 2521–2529.
- Arnold, V.I., 1984. *Catastrophe Theory*, Springer-Verlag.
- Barriere, B. & Turcotte, D.L., 1994. Seismicity and self-organized criticality, *Phys. Rev. E*, **49**, 1151–1160.
- Brace, W.F. & Byerlee, J.D., 1966. Stick-slip as a mechanism of earthquakes, *Science*, **153**, 990–992.
- Brace, W.F., Pauling, B.W. & Scholz, C.H., 1966. Dilatancy in the fracture of crystalline rocks, *J. geophys. Res.*, **71**, 3939–3953.
- Byerlee, J.D. 1967. Frictional characteristics of granite under high confining pressure, *J. geophys. Res.*, **72**, 3639–3648.
- De Santis, A., Cianchini, G., Beranzoli, L., Favali, P. & Boschi, E., 2011. The Gutenberg-Richter law and entropy of earthquakes: two case studies in central Italy, *Bull. seism. Soc. Am.*, **101**, 1386–1395.
- Dieterich, J.H., 1978a. Precursive fault slip and earthquake prediction, *J. geophys. Res.*, **83**, 3940–3947.
- Dieterich, J.H., 1978b. Time dependent friction and the mechanics of stick-slip, *Pageoph*, **116**, 790–805.
- Field, E.H. et al., 2009. Uniform California earthquake rupture forecast, Version 2 (UCERF 2), *Bull. seism. Soc. Am.*, **99**, 2053–2107.
- Field, E.H. & Page, M.T., 2011. A relatively objective, reproducible, and extensible methodology for estimating earthquake-rupture rates on a fault or fault system, *Bull. seism. Soc. Am.*, **101**, 79–92.
- Glass, L. & Mackey, M.C., 1988. *From Clocks to Chaos: The Rhythms of Life*, Princeton Univ. Press.
- Goldstein, H., 1950. *Classical Mechanics*, Addison-Wesley.
- Gutenberg, B. & Richter, C.F., 1954. *Seismicity of the Earth and Associated Phenomena*, 2nd edn, Princeton Univ. Press.
- Gutenberg, B. & Richter, C.F., 1956. Magnitude and energy of earthquakes, *Ann. Geofis.*, **9**, 1–15.
- Haken, H., 1978. *Synergetics*, Springer-Verlag.
- Hawking, S.W., 1974. Black hole explosions, *Nature*, **248**, 30–31.
- Kasahara, K., 1981. *Earthquake Mechanics*, Cambridge Univ. Press.
- Kolmogorov, A.N., 1974. *Basics of Probability Theory*, Nauka.
- Landau, L.D. & Lifshits, E.M., 1976. *Mechanics, 1, Course of Theoretical Physics*, 3rd edn, Elsevier.
- Landau, L.D. & Lifshits, E.M., 1980. Statistical Physics, Part 1, *Course of Theoretical Physics*, 3rd edn, Vol. 5, Elsevier.
- Lomnitz, C., 1974. *Global Tectonics and Earthquake Risk (Development in Geotectonics 5)*, Elsevier.
- Main, I.G. & Al-Kindy, F.H., 2002. Entropy, energy, and proximity to criticality in global earthquake populations, *Geophys. Res. Lett.*, **29**, doi:10.1029/2001GL014078.
- Main, I. & Burton, P.W., 1984. Information theory and the earthquake frequency-magnitude distribution, *Bull. seism. Soc. Am.*, **74**, 1409–1426.
- Main, I.G. & Naylor, M., 2010. Entropy production and self-organized (sub)criticality in earthquake dynamics, *Phil. Trans. R. Soc. A: Math., Phys. Eng. Sci.*, **368**, 131–144.
- Maldacena, J., 2002. *Black Holes and the Structure of Space-Time*, Public Lecture March 13, 2002, Institute for Advanced Study, Available at: www.sns.ias.edu/~malda/iaslecture3.pdf.
- Nicolis, J., 1986. *Dynamics of Hierarchic Systems: An Evolutionary Approach*, Springer-Verlag.
- Nicolis, G. & Prigogine, I., 1989. *Exploring Complexity: An Introduction*, Freeman & Co.
- Nishenko, S.P. & Buland, R., 1987. A generic recurrence interval distribution for earthquake forecasting, *Bull. seism. Soc. Am.*, **77**, 1382–1399.
- Page, R.A., Boore, D.M., Bucknam, R.C. & Thatcher, W.R., 1992. Goals, opportunities, and priorities for the USGS earthquake reduction program, U.S. Geological Survey Circular 1079.
- Parks, D.N. & Thrift, N.J., 1980. *Times, Spaces and Places; A Chronogeographic Perspective*, John Wiley and Sons.
- Pathria, R.K., 2005. *Statistical Mechanics*, 2nd edn, Elsevier.
- Poplavskaya, L.N. et al., 2006. *Regional Catalog of Sakhalin Earthquakes 1905–2005*, Yuzhno-Sakhalinsk.
- Popper, K., 1956. The arrow of time, *Nature*, **177**, 538.
- Popper, K., 1958. Irreversible processes in physical theory, *Nature*, **181**, 402.
- Prigogine, I., 1980. *From Being to Becoming: Time and Complexity in the Physical Sciences*, Freeman & Co.
- Rade, L. & Westergren, B., 2004. *Mathematics Handbook for Science and Engineering*, 5th ed., Springer-Verlag.
- Rice, J., 1980. The mechanics of earthquake rupture, in *Physics of the Earth's Interior*, pp. 555–649, eds Dziewonski, A.M. & Boschi, E., North-Holland.
- Rundle, J.B., Klein, W. & Tiampo, K.F., 2000. Linear pattern dynamics in nonlinear threshold systems, *Phys. Rev. E*, **61**, 2418–2431.
- Scholz, C.H., 1990. *The Mechanics of Earthquakes and Faulting*, 2nd edn, Cambridge Univ. Press.
- Seismic Zoning of Sakhalin (Seismicheskoe raionirovanie Sakhalina), 1977. Collection of articles, eds Solovev, S.L., Vladivostok, Akad. Nauk.
- Thom, R., 1975. *Structural Stability and Morphogenesis*, Benjamin.
- Tsuboi, C., 1956. Earthquake energy, earthquake volume, aftershock area, and strength of the earth’s crust, *J. Phys. Earthq.*, **4**, 63–66.
- Turcotte, D.L. & Schubert, G., 1982. *Geodynamics: Applications of Continuum Physics to Geological Problems*, John Wiley and Sons.
- WGCEP, 2003. Earthquake Probabilities in the San Francisco Bay Region: 2002 to 2031, Open-File Rep., U.S. Geol. Surv., 03–214.
- Wiss, M. & Brune, J.N., 1971. Regional variations of source properties in Southern California estimated from the ratio of short- to long-period amplitudes, *Bull. seism. Soc. Am.*, **61**, 1153–1167.

APPENDIX A: SEISMIC SYSTEM OF SAKHALIN

The Sakhalin SS was described in detail in (Akopian 1998; Akopian & Kocharyan 2013). This section provides a brief description of the system’s main characteristics. Seismicity and the geological characteristics of the sources of strong earthquakes in Sakhalin Island have been studied extensively in (Seismic Zoning of Sakhalin

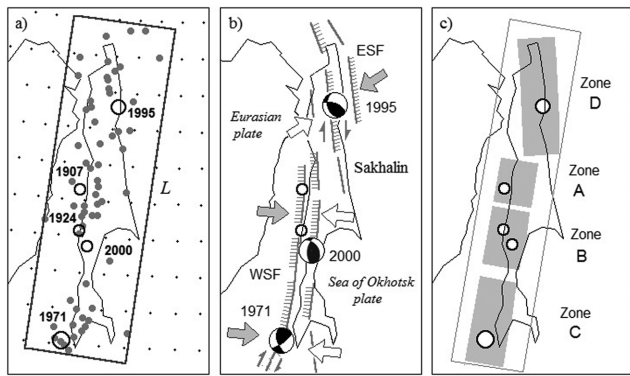


Figure A1. The Sakhalin SS: (a) Indicator earthquakes with $M \geq 5.0$ (filled circles), and configuration L of the Sakhalin SS; (b) active faults and focal mechanisms of the Moneron, Neftegorsk and Uglegorsk earthquakes. ESF and WSF are the East and West Sakhalin faults, respectively. The directions of compressive stresses are indicated by arrows: black—the thrusting plate, light—the underthrusting plate; (c) source zones of the Sakhalin SS after five strong earthquakes. Open circles in all figures denote strong earthquake epicentres with $M > 6.2$.

1977). There are five finished seismic cycles since 1907. The last cycle started in 2000, and currently the system is preparing for the next strong earthquake. The calculations were carried out on the basis of the earthquake catalogue for Sakhalin (Poplavskaya *et al.* 2006), with the additional data from the USGS/NEIC catalogue (http://www.earthquake.usgs.gov/earthquakes/eqarchives/epic/code_catalog.php). All calculations were performed on a scale of magnitude M_s . The distribution of the epicentres of shallow indicator earthquakes with magnitudes $M \geq 5.0$ for 1905–2014 allows the configuration L on the surface (which includes Sakhalin Island and the shelf) and the depth $H = 40$ km for the SS to be determined (see Fig. A1a). The SS was found by the trial-and-error method, by varying threshold magnitudes and from the boundaries of the initially selected volume of the system, chosen according to the plate-tectonic model of the region. The system configuration includes two fault systems: the West Sakhalin Fault (WSF) in the southern and central parts of the system, and the East Sakhalin Fault (ESF) in the northern part; both faults confine the epicentres of strong earthquakes (see Fig. A1b). The Eurasian and the Okhotsk Plates, which interact in the Sakhalin region along these faults, control the complex tectonic processes related to strong earthquakes in this region. Along its length of more than 1000 km, the system reaches the depth of 40 km and includes the hypocentres of crustal indicator earthquakes. Table A1 shows the data on all strong earthquakes of Sakhalin Island from 1906 to 2014. The cumulative parameters K_c and W for the seismic cycles are calculated using eqs (3), (4) and (6). In Table A1, the formulas used for energy class calculation are $K = 8.0 + 1.1 M$

at $M \geq 6.0$, and $K = 4.0 + 1.8 M$ at $M < 6.0$ (Akopian 2013b). The minimal time step δt was a month. Fig. A1c indicates the A, B, C and D zones of the Sakhalin SS, which include the epicentres of all strong earthquakes of the past. These areas determine the spatial accuracy of the prediction in the Sakhalin SS after five seismic cycles. Application of the maps of active faults enables the accurate prediction of areas where strong earthquakes are expected in the SS configuration L . Fig. A2 shows the plots of cumulative energy (3) and entropy (6) in the seismic cycles of the Sakhalin SS (contributions of aftershocks are excluded).

Fig. A3 shows the trajectory diagram of the Sakhalin SS. Its linear instability zone (seismic attractor), based on five critical points $\{W_j, K_{cj}\}, j = 1-5$, is approximated by the regression line:

$$K_c = 0.580W + 4.914 \quad W > 15.70. \quad (\text{A1})$$

Since the earthquakes in Table A1 form the attractor described by a regression line (A1), they form an ensemble of strong earthquakes for the Sakhalin SS. The extrapolation of this line to the intercept with the diagonal equilibrium line determines the minimal threshold values for indicator earthquakes: $K_h = 11.7, M_h = 4.3$ ($m_b = 4.9$). There is no direct matching between body-wave magnitude m_b and surface wave one M_s . For the Sakhalin SS, we use an approximate relation $m_b = 2.3 + 0.60 M_s$. The seismicity level of $K < 11.7$ can be considered microscopic. The sources of these weak earthquakes are distributed relatively uniformly across large areas within the Sakhalin SS. Weak earthquakes related to lower order tectonic heterogeneity (fracture) form the background seismicity, but only slightly affect the behaviour of the entire system when preparing a strong earthquake. On the trajectory diagram for the Sakhalin SS, the critical space (A, B, C, D) around the instability points of the attractor (Fig. A3) corresponds to the A, B, C and D zones on the tectonic map (see Fig. A1b,c). These areas have the average width ΔK_p and $\Delta W_p = 0.24$, which form instability areas for the tectonic zones. The prediction accuracy over time depends on the size of these zones. The concrete predictions depend on several factors: the accuracy of used catalogues, the number of finished seismic cycles, the correlation coefficient and so on. Studying the configuration of trajectories, tectonics and focal mechanisms provides a more correct interpretation for details of local sections of the attractor.

Now let us illustrate how we can predict the next strong earthquake based on the trajectory diagram in Fig. A3. The trajectory in the current time t_m (2014 January) is located above the attractor and has the coordinates ($K_{t_m} = 14.883, W_{t_m} = 16.773$). Assuming that there were no indicator earthquakes in the system after $t > t_m$

$$E_c(t) = E_c(t_m) \quad \text{for } t > t_m, \quad (\text{A2})$$

the entropy for later period of time can be found by using the following formula (Akopian & Kocharian 2013):

$$W(t_m + m) = \log[S(t_m) + mE_c(t_m)], \quad (\text{A3})$$

Table A1. Calculated seismic parameters K_{cj}, W_j in the seismic cycles of strong earthquakes for SS Sakhalin with $M_{\text{th}} = 6.2$. ξ is the energy parameter (49), η_{sc}^w is the efficiency (48). Below, parameters ϕ° and λ° are latitude and longitude, respectively (in degrees). The symbol (*) below implies a hypothetical value.

j	Data	ϕ°	λ°	K_s	M_s	K_{cj}	W_j	ξ	η_{sc}^w	Place
1	1907.01.19	50.50	141.40	15.3	6.6	14.19*	15.75*	—	—	Aleksandrovsk
2	1924.03.15	49.30	142.00	15.5	6.8	14.18	16.15	0.96	0.48 per cent	Uglegorsk
3	1971.09.05	46.25	141.20	16.3	7.5	15.24	17.67	0.93	0.12 per cent	Moneron
4	1995.05.27	52.64	142.87	15.9	7.2	14.67	16.92	0.95	0.22 per cent	Neftegorsk
5	2000.08.27	52.64	142.87	15.5	6.8	14.07	15.82	0.94	0.55 per cent	Uglegorsk
6	2014.01.01				>7.1	14.88	16.77			C or D zone

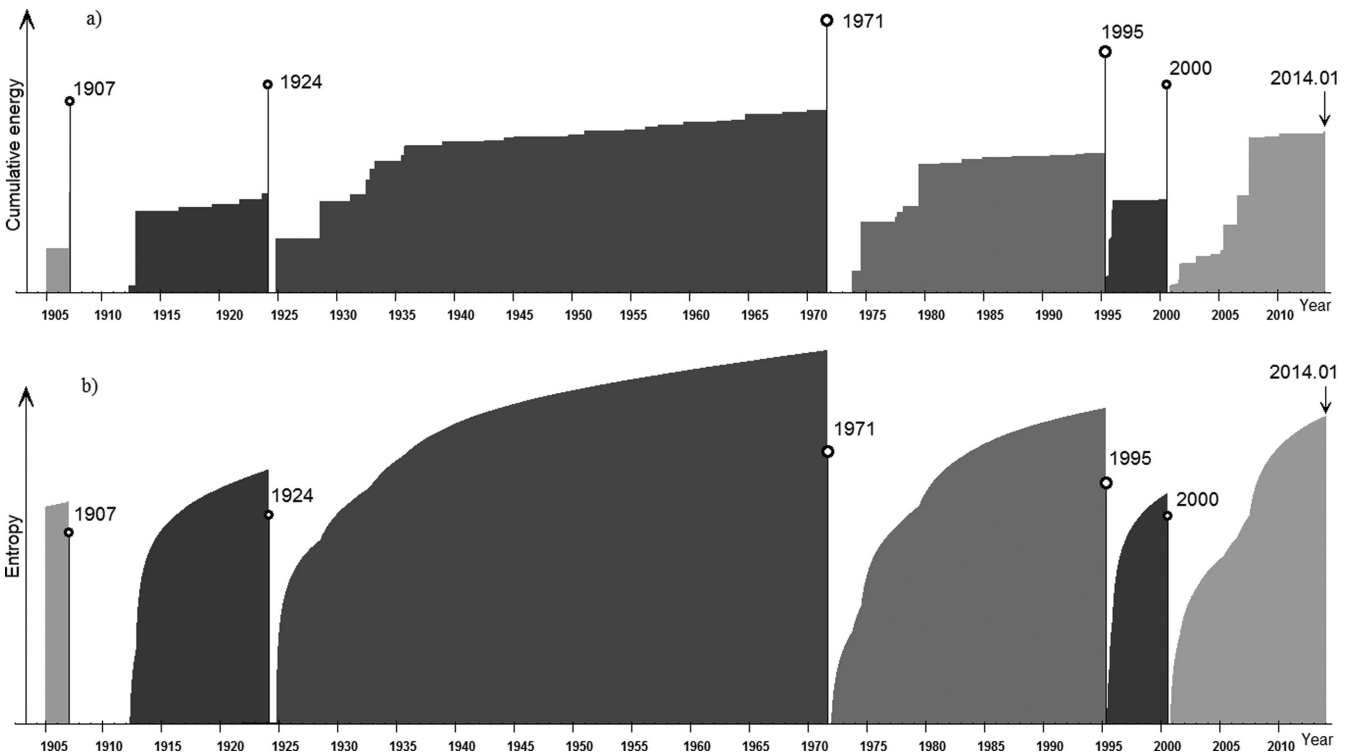


Figure A2. Graphs of cumulative energy (a) and entropy (b) in the seismic cycles of the Sakhalin SS. Points at the ends of seismic cycles denote strong earthquakes.

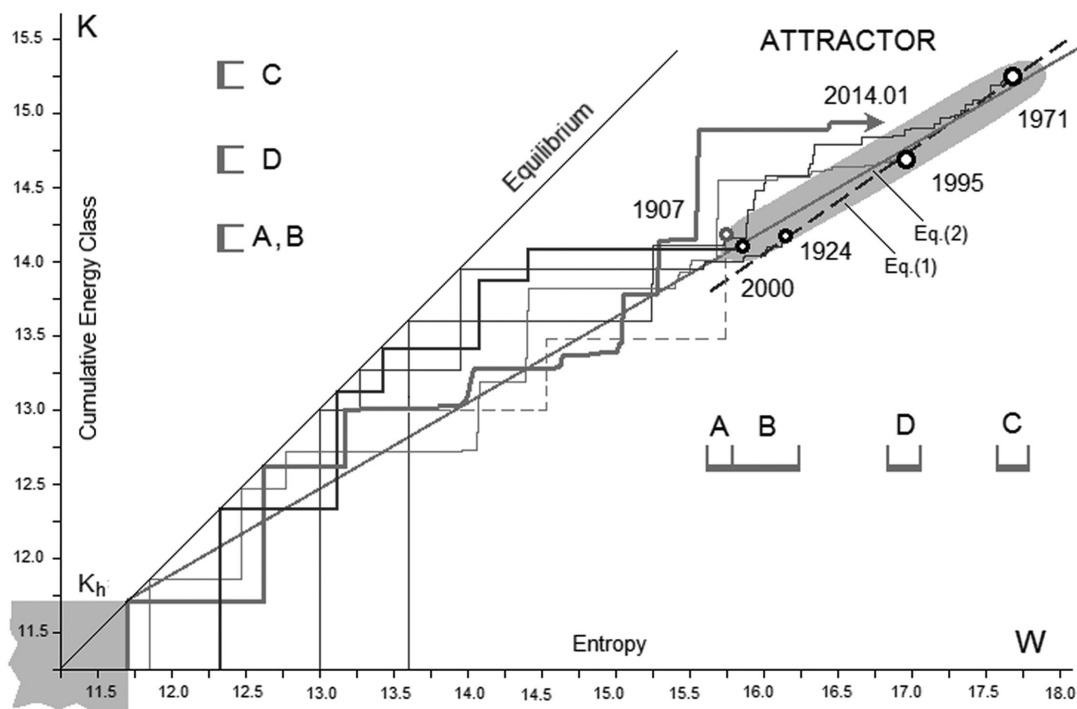


Figure A3. The trajectory diagram and attractor for the Sakhalin SS. The trajectory of current cycle (2014 January) is shown with the thick line. Curves (1) and (2) are the regression lines on three points in 1995 and on five points in 2000, respectively. The critical areas of the attractor (A, B, C, D) with respect to entropy and cumulative energy class, the equilibrium domain near the origin of coordinates ($K_h = 11.7$) and the hypothetical trajectory for the earthquake of 1907 (dotted stepwise curve) are shown.

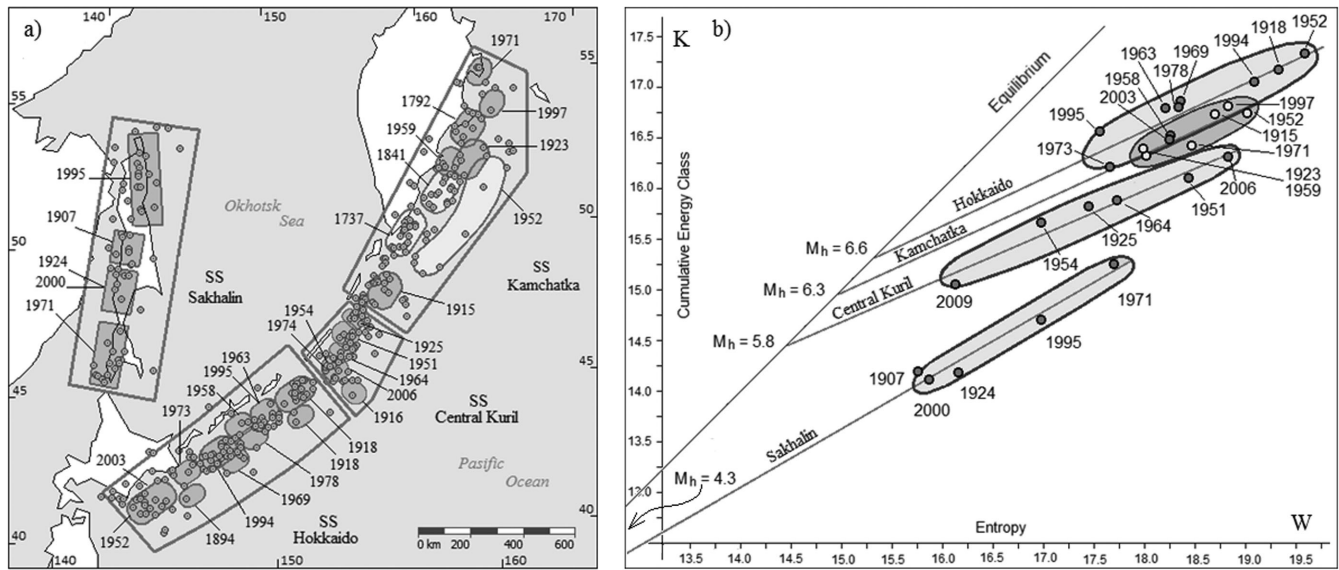


Figure B1. Kamchatka, Central Kuril, Hokkaido and Sakhalin SSs: (a) configurations, indicator earthquakes and ensembles of strong earthquakes, after (Akopian & Kocharian 2013); (b) attractors and local instability points of the strong earthquakes, are shown on the same trajectory diagram.

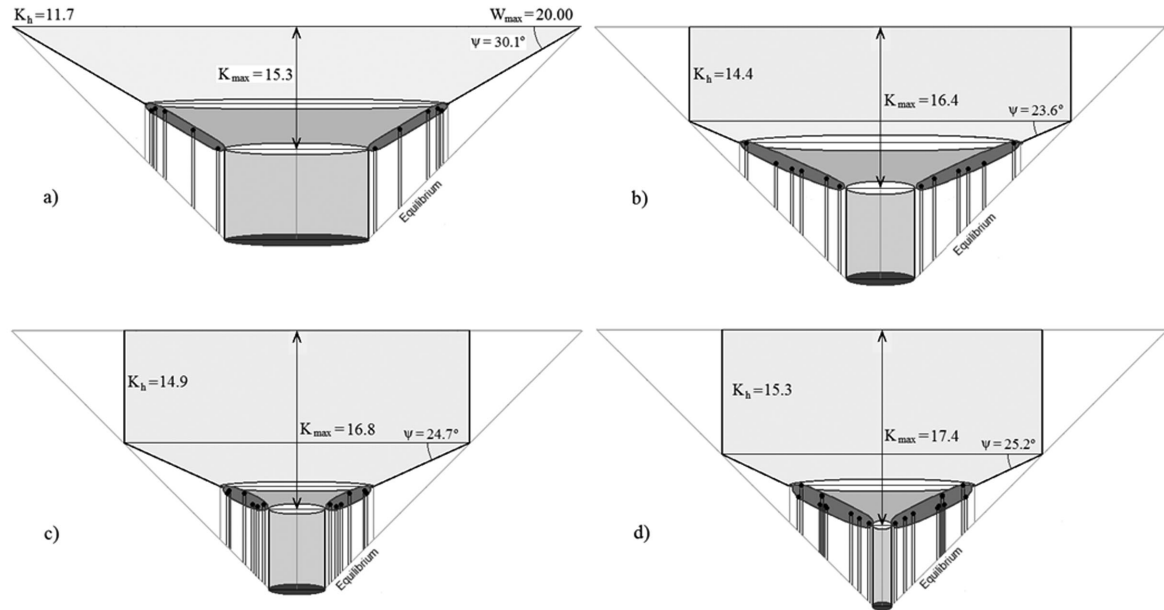


Figure B2. Entropy funnels: (a) Sakhalin SS, (b) Central Kuril SS, (c) Kamchatka SS, (d) Hokkaido SS. See notation in Section 3.1 of the main text.

where $m = 1, 2, 3, \dots$ is the ordinal number of months since current time t_m . Solving this equation, together with linear equation (36), we find the time when the trajectory reaches the intercept with the regression line (attractor):

$$m = 10^{(W_{t_m} - K_{t_m})} \left[10^{\frac{(K_{t_m} - b)}{a}} - W_{t_m} - 1 \right], \quad (\text{A4})$$

where $a = 0.580$, $b = 4.914$. According to this formula, we estimate that the next strong earthquake is to occur later than $m = 125$ months, or by 2024, in either the zone D or C. Monitoring of the entropy in the energy diagram (see Section 3.3) allows one to determine the energy (magnitude) of a predicted earthquake. Using the second eq. (44), $K_s = 0.456W_{t_m} + 8.208$ and $K_s = 8.0 + 1.1 M_s$, we find that the predicted magnitude at the current time is $M_s \simeq 7.1$. According to

the formula (A3), we find that 125 months later the entropy value will increase to $W(t_m + 125) = 17.190$ and the magnitude of an earthquake expected in year 2024 increases to $M_s \simeq 7.3$.

APPENDIX B: ENTROPY FUNNELS OF SEISMIC SYSTEMS

Configurations, indicator earthquakes and ensembles of strong earthquakes for the Sakhalin, Central Kuril, Kamchatka and Hokkaido SSs are given in Fig. B1(a). The attractors for these systems are combined on a trajectory diagram (Fig. B1b). Attractors include the instability points for ensembles of strong earthquakes and the threshold magnitudes M_h of an equilibrium indicator earthquake. The regression equations of attractors for these systems are

written in the following form:

$$K = 0.580W + 4.937 \text{ Sakhalin}, \quad (\text{B1})$$

$$K = 0.436W + 8.160 \text{ Central Kuril}, \quad (\text{B2})$$

$$K = 0.460W + 8.071 \text{ Kamchatka}, \quad (\text{B3})$$

$$K = 0.470W + 8.113 \text{ Hokkaido}. \quad (\text{B4})$$

Vertical cross-sections of entropy funnels are shown in Fig. B2 in the same scale for the Sakhalin, Central Kuril, Kamchatka, and Hokkaido SSs. The maximal value of entropy for all funnels is assumed equal $W_{\max} = 20.00$, notation is the same as Fig. 16(b). Trajectories are drawn into the funnel at $K > K_h$ and leave the funnels to attain the equilibrium state through annular instability zones of ensembles of strong earthquakes. As threshold magnitudes grow, entropy funnels become deeper and narrower.